Figure 2. The pupillary light reflex (PLR) to monochromatic light stimulation, as measured in 10 GD patients and controls. Each trace was elicited by a red (A) or blue (B) single flash stimulus, with duration of 1 sec and intensity of 100 cd/m^2. (A) Red light-induced PLRs were normal in P1 (GD1: non-neuronopathic type) but markedly attenuated or absent in neuronopathic GD patients (P2–6: type 2, P7–10: type 3) except for P2. (B) Blue light-induced PLRs were normal in P1 and relatively spared in GD2 patients but absent in GD3 patients (except for P7). The mean measurements of initial constriction rate (CR) are shown in Table 1.

clear waveforms were confirmed in only one patient (Patient 2); the remaining three patients showed significantly low R-CRs. In contrast, blue light-induced CRs (B-CRs) were relatively spared. All neuronopathic patients already exhibited horizontal saccadic initiation failure at initial PLR examination. Patient 1 (GD1) had no abnormalities in all assessments.

Discussion

In this study, we successfully used pupillometry to identify PLR impairment in neuronopathic GD patients. We

noted that the qualitative trend for reduced R-CRs was associated with the severity of the neurological symptoms, as indicated by activity of daily living (ADL) deficits. Our findings suggest that neuronopathic GD progression induces severe attenuation of R-CR, with relative sparing of B-CR. To our knowledge, the abnormal PLR in neuronopathic GD is a novel physiological finding.

The PLR pathway begins with the axons of photosensitive retinal ganglion cells (RGCs) that convey information to the optic nerve. The optic nerve subsequently connects to several targets in the midbrain, including the olivary pretectal nucleus (OPN) and Edinger–Westphal nucleus (EWN), and the oculomotor nerve. Neuronopathic GD is known to involve the midline of the dorsal brainstem, EWN, and oculomotor nucleus.[10–12] Thus, it is possible that PLR abnormalities may reflect dysfunctional parasympathetic innervation between the dorsal midline of the midbrain and the iris. However, the physiology that underlies the difference between R-CR and B-CR remains unclear. These findings led us to propose two hypotheses: (1) relative sparing of B-CR may be derived from the function of ipRGCs; (2) functional changes of the inner retina may lead to loss of R-CR.

For decades, rods and cones were considered the only photoreceptors, and both provide excitatory input to conventional RGCs via bipolar cells. However, the discovery of ipRGCs and the presence of the characteristic photopigment melanopsin in them have led to changes in this classical view.[13,14] Melanopsin-expressing ipRGCs comprise 0.2% RGCs and respond to light stimulation in the absence of any synaptic rod/cone input.[15] The ipRGCs combine their direct photoresponses with synaptic rod/cone input and project to several brain nuclei that regulate circadian rhythms (the suprachiasmatic nucleus), PLR (OPN) and the imaging-forming system (the lateral geniculate nucleus). However, little is known about the differences in the pathways of conventional RGCs and ipRGCs in the optic nerve and brainstem.

Recently, increasing evidence has indicated that ipRGCs are resistant to neurodegeneration. Histopathological studies in patients with mitochondrial optic neuropathy have shown relative sparing of ipRGCs compared with conventional RGCs,[16] with pupillometry analysis showing a slight reduction in CR in the affected eye.[17] In addition, only ~17% ipRGCs need to be activated to drive full pupillary constriction in ipRGC-knockout mice.[18] Thus, we speculate that ipRGCs likely have a high cellular resistance to metabolic derangement, leading to relative preservation of B-CR.

Next, we investigated why neuronopathic GD patients show R-CR impairment even though their rods and cones remain functional. Several prior studies have suggested the utility of chromatic pupillometry to monitor each photoreceptor separately using stimuli of different wavelengths and

Table 1. Genotypes, phenotypes, and clinical findings of GD patients.

ID	Sex	Age at onset of HSIF	Age at PLR exam	Phenotype	Genotype	ADL	Communication	R-CR (%)	B-CR (%)	Visual acuity	SIF	PF	Vertical gaze palsy	VOR	VEP	ERG
1	M	(−)	24 years	1	L444P/D409H	N	N	28.8	46.8	N	(−)	(−)	(−)	(+)	N	N
2	M	7 months	7 months	2	F213I/R120W	N	N	22.7	55.0	N	(+)	(+)	(−)	(+)	N	N
3	F	6 months	7 months	2	V230G/R296X	B/Tra/Tu	I	15.0	44.5	NA	(+)	(+)	(+)	NA	NA	N
4	F	3 months	9 months	2	L444P/R120W	B/Tra/Tu/V	I	5.5	40.0	NA	(+)	(+)	(+)	(−)	Giant VEP	OPs↓
5	F	?	2 years	2	RecNciI/?	B/Tra/Tu/V	I	(−)	44.7	NA	(+)	(+)	(+)	(−)	N	OPs↓
6	F	2 months	3 years	2	F213I/RecNciI	B/Tra/Tu/V	I	(−)	38.8	NA	(+)	(+)	(+)	(−)	Giant VEP	OPs↓
7	F	8 months	9 years	3	L444P/L444P	N	N	7.0	51.0	N	(+)	(+)	(−)	(−)	N	N
8	F	16 years	16 years	3	N188S/?	TA	N	(−)	(−)	N	(+)	(−)	(−)	Fast phase (−)	N	N
9	F	20 years	20 years	3	N188S/?	TA	N	(−)	(−)	N	(+)	(−)	(−)	Fast phase (−)	Giant VEP	N
10	F	14 years	29 years	3	N188S/ G193W	B/Tra/Tu	I	(−)	(−)	NA	(+)	(+)	(+)	(−)	Giant VEP	N
Control 1 (n = 30)	Median age: 23 years (range: 22 – 37 years, M:F = 9:13)							35.1 ± 7.0	48.1 ± 5.6							
Control 2	4 years (F)							45.0	56.0							
Control 3	6 years (F)							38.0	53.5							

F, female; M, male; HSIF, horizontal saccadic initiation failure; PLR, pupillary light reflex; ADL, activity of daily living; N, normal or age-appropriate; B, bedridden; Tra, tracheotomy; V, ventilation; Tu, tube feeding; TA, total assistance; I, impaired; R-CR, red light-induced initial constriction rate; B-CR, blue light-induced initial constriction rate; (−), negative construction (CR < 5%); SIF, saccadic initiation failure; PF, pursuit failure; VOR, vestibulo-ocular reflex; ERG, electroretinogram; VEP, visual evoked potential; NA, not available; OPs, oscillatory potentials; ↓, attenuated.

intensities.[8,9,19] M/L cones can be uniquely stimulated at wavelengths beyond 620 nm (red light, λ_{max} = 543, 566 nm), whereas other photoreceptors are thought to be insensitive. Rods respond to blue light (λ_{max} = 507 nm) at low luminance levels (normal threshold at -3 to -5 log cd/m^2) and ipRGCs are sensitized to blue light (λ_{max} = 482 nm) at higher luminance levels (100 cd/m^2).

In this study, we selected high-intensity blue and red stimuli to sensitize ipRGCs and L/M cones. Although all patients exhibited normal a-wave amplitudes with flash-ERG, which reflects cone activity, R-CR was severely impaired. On the other hand, decreased ERG OPs were found in our patients and decreased ERG b-wave amplitudes have been reported in a visually asymptomatic GD patient.[20] Lowering OPs and b-wave amplitudes are typically attributed to changes in the inner nuclear layer (amacrine cells and Müller cells) of the retina.

Therefore, we assume that the primary deficit (storage of substrate) caused secondary functional changes to the inner retina, and the synaptic rod/cone inputs to both RGCs via bipolar cells may be blocked, resulting eventually in the progression of R-CR (derived from cone/rod activation via conventional RGCs and ipRGCs) to loss. On the other hand, B-CR may be relatively spared because of their intrinsic response of ipRGCs. While further studies are warranted, chromatic pupillometry can be used to facilitate future investigation of GD pathophysiology.

In conclusion, neuronopathic GD patients have PLR impairments and chromatic pupillometry appears to be a useful method to evaluate such patients, regardless of age or neurocognitive status. Further studies are required to investigate the utility of this method to monitor prognosis and as a predictor of disease progression in larger patient samples.

Acknowledgment

Author Contribution

Kentarou Shirai, M.D., Koyo Ohno, M.D., Yoko Nishimura, M.D., and Akiko Tamasaki, M.D. were involved in examining the patients and collecting the resulting data. Norika Kubota, Ph.D., M.D., Rumiko Takayama, M.D., Yukitoshi Takahashi, Ph.D., M.D., Takanori Onuki, M.D., Chikahiko Numakura, Ph.D., M.D., Mitsuhiro Kato, Ph.D., M.D., Yusuke Hamada, M.D., Norio Sakai, Ph.D., M.D., Atsuko Ohno, M.D., Maya Asami, M.D., Shoko Matsushita, Ph.D., M.D., Anri Hayashi, M.D., Tomohiro Kumada, Ph.D., M.D., Tatsuya Fujii, Ph.D., M.D., Asako Horino, M.D., and Takeshi Inoue, M.D., Ichiro Kuki, M.D. were responsible for introducing the patients to our hospital and actively involved in the methods employed for the purpose of this study. Ken Asakawa, Ph.D., Hitoshi Ishikawa, Ph.D., M.D., Yoshihiro Maegaki, Ph.D., M.D., and Kousaku Ohno, Ph.D., M.D. supervised the entire study, providing value inputs for the methods and discussion aspects of the manuscript.

Conflict of Interest

None declared.

References

1. Scriver CR. The metabolic and molecular bases of inherited disease. 7th ed. New York: McGraw-Hill, Health Professions Division, 1995.
2. Tylki-Szymanska A, Vellodi A, El-Beshlawy A, et al. Neuronopathic Gaucher disease: demographic and clinical features of 131 patients enrolled in the International Collaborative Gaucher Group Neurological Outcomes Subregistry. J Inherit Metab Dis 2010;33:339–346.
3. Patterson MC, Horowitz M, Abel RB, et al. Isolated horizontal supranuclear gaze palsy as a marker of severe systemic involvement in Gaucher's disease. Neurology 1993;43:1993–1997.
4. Harris CM, Taylor DS, Vellodi A. Ocular motor abnormalities in Gaucher disease. Neuropediatrics 1999;30:289–293.
5. Kardon R, Anderson SC, Damarjian TG, et al. Chromatic pupillometry in patients with retinitis pigmentosa. Ophthalmology 2011;118:376–381.
6. Kawasaki A, Crippa SV, Kardon R, et al. Characterization of pupil responses to blue and red light stimuli in autosomal dominant retinitis pigmentosa due to NR2E3 mutation. Invest Ophthalmol Vis Sci 2012;53:5562–5569.
7. Ishikawa H, Onodera A, Asakawa K, et al. Effects of selective-wavelength block filters on pupillary light reflex under red and blue light stimuli. Jpn J Ophthalmol 2012;56:181–186.
8. Kardon R, Anderson SC, Damarjian TG, et al. Chromatic pupil responses: preferential activation of the melanopsin-mediated versus outer photoreceptor-mediated pupil light reflex. Ophthalmology 2009;116:1564–1573.
9. Park JC, Moura AL, Raza AS, et al. Toward a clinical protocol for assessing rod, cone, and melanopsin contributions to the human pupil response. Invest Ophthalmol Vis Sci 2011;52:6624–6635.
10. Buttner-Ennever JA, Uemura T, Arai Y, et al. Horizontal saccadic palsy associated with gliosis of the brainstem midline. Prog Brain Res 2008;171:597–603.
11. Kaga K, Ono M, Yakumaru K, et al. Brainstem pathology of infantile Gaucher's disease with only wave I and II of

auditory brainstem response. J Laryngol Otol 1998;112:1069–1073.

12. Grafe M, Thomas C, Schneider J, et al. Infantile Gaucher's disease: a case with neuronal storage. Ann Neurol 1988;23:300–303.

13. Qiu X, Kumbalasiri T, Carlson SM, et al. Induction of photosensitivity by heterologous expression of melanopsin. Nature 2005;433:745–749.

14. Hattar S, Kumar M, Park A, et al. Central projections of melanopsin-expressing retinal ganglion cells in the mouse. J Comp Neurol 2006;497:326–349.

15. Dacey DM, Liao HW, Peterson BB, et al. Melanopsin-expressing ganglion cells in primate retina signal colour and irradiance and project to the LGN. Nature 2005;433:749–754.

16. La Morgia C, Ross-Cisneros FN, Sadun AA, et al. Melanopsin retinal ganglion cells are resistant to neurodegeneration in mitochondrial optic neuropathies. Brain 2010;133:2426–2438.

17. Kawasaki A, Herbst K, Sander B, et al. Selective wavelength pupillometry in Leber hereditary optic neuropathy. Clin Experiment Ophthalmol 2010;38:322–324.

18. Guler AD, Ecker JL, Lall GS, et al. Melanopsin cells are the principal conduits for rod-cone input to non-image-forming vision. Nature 2008;453: 102–105.

19. Markwell EL, Feigl B, Zele AJ. Intrinsically photosensitive melanopsin retinal ganglion cell contributions to the pupillary light reflex and circadian rhythm. Clin Exp Optom 2010;93:137–149.

20. Seidova SF, Kotliar K, Foerger F, et al. Functional retinal changes in Gaucher disease. Doc Ophthalmol 2009;118:151–154.

140

Human Bocavirus in Patients with Encephalitis, Sri Lanka, 2009–2010

Daisuke Mori, Udaya Ranawaka,
Kentaro Yamada, Shaman Rajindrajith,
Kazushi Miya, Harsha Kumara Kithsiri Perera,
Takashi Matsumoto, Malka Dassanayake,
Marcelo Takahiro Mitui, Hisashi Mori,
Akira Nishizono, Maria Söderlund-Venermo,
and Kamruddin Ahmed

We identified human bocavirus (HBoV) DNA by PCR in cerebrospinal fluid from adults and children with encephalitis in Sri Lanka. HBoV types 1, 2, and 3 were identified among these cases. Phylogenetic analysis of HBoV1 strain sequences found no subclustering with strains previously identified among encephalitis cases in Bangladesh.

Encephalitis is a serious infection causing high rates of illness and, in industrialized countries, has a case-fatality rate of 6.5%–12% (1,2). However, the situation in developing countries is largely unknown. Globally, the causes remain unrecognized in 60%–85% of encephalitis cases (1,2). Recently, human bocavirus (HBoV) has been implicated in causing life-threatening encephalitis in Bangladeshi children (3). In Sri Lanka, information about the causative agents of encephalitis is scarce. The aim of this study was to determine the occurrence of HBoV and other possible pathogens in children and adults with encephalitis admitted to a tertiary care hospital in Sri Lanka.

The Study

The study was conducted at Colombo North Teaching Hospital, Ragama, Sri Lanka, during July 2009–November 2010. A total of 233 patients (110 adolescents/adults ≥12 years of age and 123 children) were enrolled. Adolescents and adults were admitted to adult wards. Cerebrospinal fluid (CSF) samples were available from 191 patients.

Author affiliations: Oita University, Yufu, Japan (D. Mori, K. Yamada, T. Matsumoto, M.T. Mitui, A. Nishizono, K. Ahmed); University of Kelaniya, Ragama, Sri Lanka (U. Ranawaka, S. Rajindrajith, H.K.K. Perera); Colombo North Teaching Hospital, Ragama (M. Dassanayake); University of Toyama, Toyama, Japan (K. Miya, H. Mori); and University of Helsinki, Helsinki Finland (M. Söderlund-Venermo)

Criteria for enrolment were as follows: any combination of the triad of fever, headache, and vomiting, along with altered level of consciousness, seizures, focal neurologic deficits, altered behavior, and signs of meningeal irritation. Clinical and laboratory information was available for 164 patients. The male:female ratio for adolescents/adults was 1.3:1; ages ranged from 12 to 90 years (mean 42 years); For children, the male:female ratio was 0.7:1; ages ranged from 2 to 144 months (mean 48 months). The ethics committees of the University of Kelaniya and Oita University approved this study.

CSF samples were subjected to macroscopic examination, total and differential leukocyte counts, bacterial culture, Gram staining, and measurement of protein and glucose. Blood was cultured for bacteria and examined for total and differential leukocyte counts, erythrocyte sedimentation rates, and hemoglobin and C-reactive protein levels.

Classical encephalitis-causing pathogens (Table) and diarrheagenic viruses, such as HBoV, rotavirus, astrovirus, norovirus, parechovirus, and human adenovirus (HAdV), were determined in CSF by PCR (online Technical Appendix, wwwnc.cdc.gov/EID/articlepdfs/19/11/12-1548-Techapp1.pdf) (3–5). Anti-N-methyl-D-aspartate receptor (NMDAR) encephalitis was diagnosed by on-cell Western analysis (6). For HBoV PCR-positive patients, HBoV types 1–4-specific IgG and IgM responses in CSF samples were measured by enzyme immunoassays (7).

Nucleotide sequences of all amplicons were determined to confirm the PCR products, to distinguish genotypes, and to perform phylogenetic analysis (3). BLAST analysis (www.ncbi.nlm.nih.gov/blast) was used to identify the viruses and genotypes. Multiple sequence alignment was conducted by using ClustalW2 (www.ebi.ac.uk/clustalw). The phylogenetic analysis was done with a neighbor-joining tree by using MEGA5 (www.megasoftware.net). A bootstrap analysis of 1,000 replicates was performed to test the reliability of the branching pattern.

The causes of encephalitis were type 2 dengue virus in 1 (0.5%) patient, human echovirus (HEcoV) type 9 or 25 in 2 (1%), HBoV (Table) in 5 (3%), and HAdV 41 in 7 (4%): all were sole detections. None of the other viruses and no bacteria were detected. Samples positive for HBoV by primers designed from viral protein 1/2 also were positive by primers designed from nonstructural protein (NP) 1 gene. HEcoV was detected in 2- and 9-year-old children. HAdV 41 was not confined to children; ages of infected patients ranged from 13 months to 55 years. Of 81 CSF samples, anti-NMDAR encephalitis was detected in 2 (2%) adults (42 and 72 years of age). All patients in this study recovered and were discharged, except for one 13-month-old boy with HAdV 41 encephalitis who left the hospital against medical advice.

Table. Characteristics of patients with HBoV encephalitis, Sri Lanka, 2009–2010*

Characteristic	93018	56684	84770	64502	285
Virus in CSF					
Virus detected†	HBoV1	HBoV1	HBoV1	HBoV2	HBoV3
HBoV IgM and IgG	Neg	Neg	Neg	Neg	Neg
Patient demographic					
Sex	F	F	M	M	F
Age	66 y	46 y	5 mo	17 y	8 mo
Place of residence	Kaleliya	Wattala	Mirigama	Makola	Heiyanthiduwa
Hospitalization					
Time between illness onset and hospitalization	NA	48 h	24 h	48 h	48 h
Duration of hospitalization	7 d	4 d	12 d	4 d	3 d
CSF test result‡					
Color	Clear	Clear	Clear	Clear	Clear
Leukocyte count, cells/μL	1	0	380	0	0
PMNs	0	0	130	0	0
Lymphocytes	1	0	250	0	0
Protein, mg/dL	NA	113	170	38	25
Glucose, mg/dL	65	160	48	63	83
Results of Gram stain	Neg	Neg	ND	Neg	Neg
Bacterial culture	ND	ND	Neg	ND	ND
Blood tests§					
Leukocyte count, cells/μL	10,000	15,200	36,500	15,900	13,200
PMNs, %	63.2	70	62	ND	52
Lymphocytes, %	21.6	21	35	ND	47
Hemoglobin, g/dL	12.2	12	7.7	13.2	13.2
ESR, mm/h	27	68	ND	ND	ND
CRP, mg/dL	ND	ND	>12	ND	<6
Glasgow coma score <15	No	Yes, 12	No	No	No
Outcome	Discharged	Discharged	Discharged	Discharged	Discharged

*HBoV, human bocavirus; CSF, cerebrospinal fluid; Neg, negative; NA, not available; PMN, polymorphonuclear neutrophil: ND, not done; ESR, erythrocyte sedimentation rate; CRP, C-reactive protein.
†The following viruses were tested for herpes simplex virus (HSV) type 1, HSV-2, varicella-zoster virus (HSV-3), Epsetin-Barr virus (human herpesvirus [HHV] type 4), cytomegalovirus (HHV-5), (HHV-6), HHV-7, HHV-8, dengue virus, Japanese encephalitis virus, rubella virus, West Nile virus, yellow fever virus, tick-borne encephalitis virus, Nipah virus, measles virus, mumps virus, parainfluenza virus, respiratory syncytial virus, metapneumovirus, Chikungunya virus, Sindbis virus, Semliki Forest virus, eastern equine encephalitis virus, western equine encephalitis virus, poliovirus, Coxsackie virus, echovirus, enterovirus, lyssaviruses, and Chandipura virus. Bacteria were tested by PCR amplification of 16S rRNA, followed by sequencing.
‡Reference values: leukocyte count <5 cells/mm³ and all lymphocytes; PMNs, none; protein, 20–45 mg/dL; glucose, 50–80 mg/dL or >50% of blood glucose level.
§Reference values: leukocyte count, 4,000–11,000 cells/mm³; PMNs, 40–60% of leukocyte count; lymphocytes, 20%–40% of leukocyte count; hemoglobin, men: 14–18 g/dL, women, (12–15 g/dL, children: 11–16 g/dL; ESR, <20 mm in1st hr., CRP, <12 mg/dL.

The severity of symptoms in the HBoV-positive patients did not differ from those of patients with other infections. None of the patients who had positive PCR results for HBoV1–3 had corresponding HBoV1–4 IgM or IgG in their CSF. Phylogenetic analysis (Figure) of the viral protien 1/2 gene showed that the Sri Lanka HBoV1 strains did not subcluster with encephalitis-associated Bangladesh strain, although they had 97%–98% nt identities. The Sri Lanka HBoV1 strains had 98%–99% nt identities among themselves and with other HBoV1 strains. The Sri Lanka HBoV2 strain was closely related to the Tunisia strain (96% nt identity). The Sri Lanka HBoV2 had 90%–91% nt identities with the Bangladeshi encephalitis-causing strains and 90%–96% nt identities with other HBoV2 strains. The Sri Lanka HBoV3 strain was closely associated with the cluster formed by viruses from the United Kingdom, Australia, Tunisia, and China and had 96%–97% nt identities with those strains. The sequence of NP1 gene is conserved and had 98%–100% nt identities among the Sri Lanka strains.

Conclusions

The study in Bangladesh suggested that HBoV-associated encephalitis might be restricted to malnourished children (3). However, our study demonstrates that HBoV also can be detected in well-nourished children and adults with encephalitis. How HBoV might trigger encephalitis is unclear. HBoV viremia has been documented, and the virus might therefore have the potential to cross the blood–brain barrier. The NP1 of HBoV inhibits interferon-β production by the host, suggesting evasion of the innate immune response during infection (8).

Unlike the Bangladesh study, where 2 of 4 encephalitis patients in whom HBoV was detected died (3), all patients in our study recovered. In addition to HBoV1 and HBoV2, we detected HBoV3 in a child with encephalitis, which to our knowledge, has not been reported as a cause of the disease. Although HBoV infections occur mainly in children, among the 5 Sri Lanka patients with HBoV encephalitis, 3 were adults or adolescents. None of the patients with HBoV encephalitis had HBoV IgM or IgG in their CSF, indicating
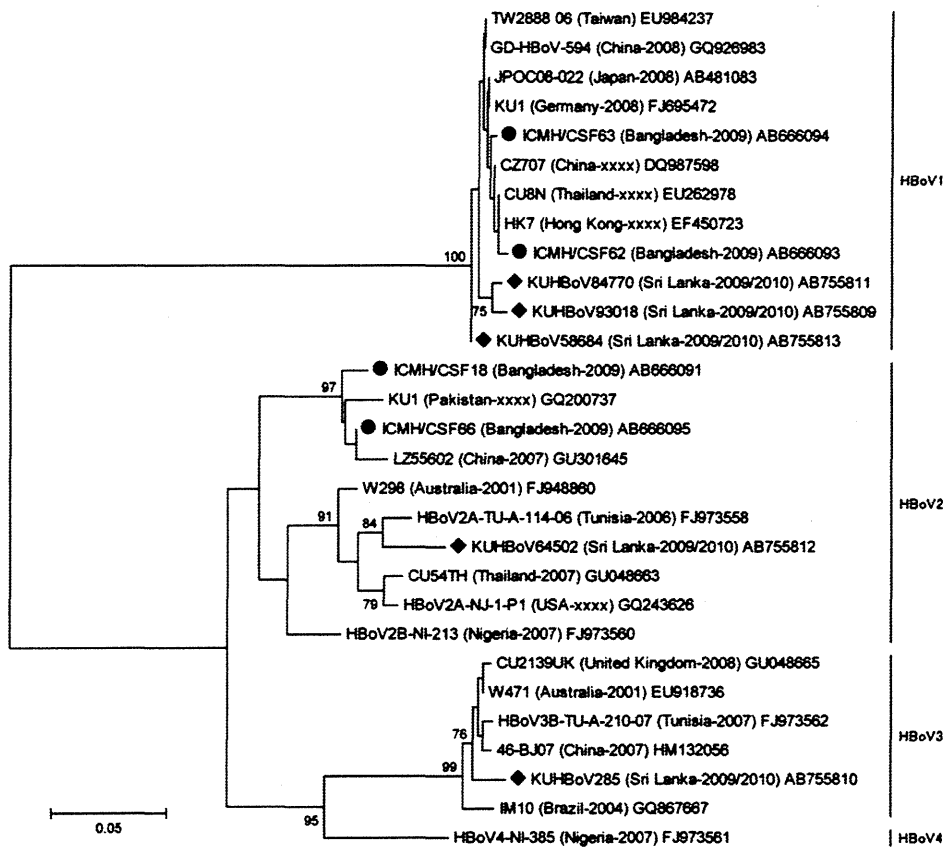
TW2888 06 (Taiwan) EU984237

GD-HBoV-594 (China-2008) GQ926983

JPOC08-022 (Japan-2008) AB481083

KU1 (Germany-2008) FJ695472

● ICMH/CSF63 (Bangladesh-2009) AB666094

CZ707 (China-xxxx) DQ987598

CU8N (Thailand-xxxx) EU262978

HK7 (Hong Kong-xxxx) EF450723

● ICMH/CSF62 (Bangladesh-2009) AB666093

◆ KUHBoV84770 (Sri Lanka-2009/2010) AB755811

◆ KUHBoV93018 (Sri Lanka-2009/2010) AB755809

◆ KUHBoV58684 (Sri Lanka-2009/2010) AB755813

● ICMH/CSF18 (Bangladesh-2009) AB666091

KU1 (Pakistan-xxxx) GQ200737

● ICMH/CSF66 (Bangladesh-2009) AB666095

LZ55602 (China-2007) GU301645

W298 (Australia-2001) FJ948860

HBoV2A-TU-A-114-06 (Tunisia-2006) FJ973558

◆ KUHBoV64502 (Sri Lanka-2009/2010) AB755812

CU54TH (Thailand-2007) GU048663

HBoV2A-NJ-1-P1 (USA-xxxx) GQ243626

HBoV2B-NI-213 (Nigeria-2007) FJ973560

CU2139UK (United Kingdom-2008) GU048665

W471 (Australia-2001) EU918736

HBoV3B-TU-A-210-07 (Tunisia-2007) FJ973562

46-BJ07 (China-2007) HM132056

◆ KUHBoV285 (Sri Lanka-2009/2010) AB755810

IM10 (Brazil-2004) GQ867667

HBoV4-NI-385 (Nigeria-2007) FJ973561

HBoV1, HBoV2, HBoV3, HBoV4

100, 97, 91, 84, 79, 75, 76, 99, 95

0.05

Figure. Phylogenetic tree of the partial VP 1/2 gene (nucleotide positions 3233–3808, amplicon size 575 bp) of HBoVs constructed by using nucleotide sequence by neighbor-joining method. The strain name is followed by country of origin and year of sample collection in parentheses, followed by the DDBJ/EMBL/GenBank accession no.; xxx indicates that the year of sample collection is undocumented. Sri Lanka and Bangladesh encephalitis-causing bocaviruses are indicated by circles and diamonds, respectively. The number adjacent to the node represents the bootstrap value, and values <70% are not shown. Scale bar indicates genetic distance expressed as nucleotide substitutions per site. (The DDBJ/EMBL/GenBank accession numbers of nonstructural protein 1 gene of strains KUHBoV93018, KUHBoV285, KUHBoV84770, KUHBoV64502 and KUHBoV58684 were AB822999, AB823000, AB823001, AB823002 and AB823003, respectively).

how rapidly disease onset occurred and how little time the immune system had to respond. Generally, the specific seroprevalence rate of HBoV1 antibodies in infected persons is 59%, followed by HBoV2, 3, and 4 (34%, 15%, and 2%, respectively) (7).

Our detection rate of viruses as a cause of encephalitis was 7.5%, and adding anti-NMDAR encephalitis, the detection rate increased to 10%, which is similar to that of another study (9). Anti-NMDAR encephalitis is becoming a dominant cause of encephalitis in certain population (10); however, in Sri Lanka, it is 1%–4%, similar to other studies (11).

Dengue virus is the leading endemic cause of encephalitis in Brazil (12). This infection is also endemic to Sri Lanka and, before our study, dengue encephalitis was suspected but unconfirmed in the population. Enteroviruses frequently cause CNS infection, and the HEcoV 9 and 25 found here are known to cause encephalitis (13).

Among the HAdVs, serotype F is mainly responsible for gastroenteritis, whereas encephalitis is caused mainly by serotypes B, C, and D (14,15). The large number of HAdV 41 encephalitis cases indicates a unique epidemiology in Sri Lanka.

Herpes simplex and varicella-zoster viruses are implicated as the major causes of encephalitis. However, these viruses were not responsible for encephalitis in our study or in the studies in Bangladesh. HBoV is dominant in both Bangladesh and Sri Lanka. The limitation of our study is that causation could not be proven by the presence of HBoV antibody during infection or the absence of HBoV DNA in the CSF when recovered. The HBoV DNA detected in our study may represent persistent DNA from past infection; however, history of recent respiratory or diarrheal infection was absent. Future studies using quantitative PCR and serology are warranted to better establish the etiologic role of HBoV infection and encephalitis.

Mr Mori is a medical technologist and is enrolled in the PhD program in the Department of Microbiology, Faculty of Medicine, Oita University, Japan. His research interest is molecular epidemiology of viruses.

References

1. Granerod J, Ambrose HE, Davies NW, Clewley JP, Walsh AL, Morgan D, et al. Causes of encephalitis and differences in their clinical presentations in England: a multicentre, population-based prospective study. Lancet Infect Dis. 2010;10:835–44. http://dx.doi.org/10.1016/S1473-3099(10)70222-X

2. Huppatz C, Durrheim DN, Levi C, Dalton C, Williams D, Clements MS, et al. Etiology of encephalitis in Australia, 1990–2007. Emerg Infect Dis. 2009;15:1359–65. http://dx.doi.org/10.3201/eid1509.081540

3. Mitui MT, Shahnawaz Bin Tabib SM, Matsumoto T, Khanam W, Ahmed S, Mori D, et al. Detection of human bocavirus in the cerebrospinal fluid of children with encephalitis. Clin Infect Dis. 2012;54:964–7. http://dx.doi.org/10.1093/cid/cir957

4. Han TH, Kim CH, Park SH, Chung JY, Hwang ES. Detection of human parechoviruses in children with gastroenteritis in South Korea. Arch Virol. 2011;156:1471–5. http://dx.doi.org/10.1007/s00705-011-0995-y

5. Allander T, Tammi MT, Eriksson M, Bjerkner A, Tiveljung-Lindell A, Andersson B. Cloning of a human parvovirus by molecular screening of respiratory tract samples. Proc Natl Acad Sci U S A. 2005;102:12891–6. http://dx.doi.org/10.1073/pnas.0504666102

6. Takano S, Takahashi Y, Kishi H, Taguchi Y, Takashima S, Tanaka K, et al. Detection of autoantibody against extracellular epitopes of N-methyl-D-aspartate receptor by cell-based assay. Neurosci Res. 2011;71:294–302. http://dx.doi.org/10.1016/j.neures.2011.07.1834

7. Kantola K, Hedman L, Arthur J, Alibeto A, Delwart E, Jartti T, et al. Seroepidemiology of human bocaviruses 1–4. J Infect Dis. 2011;204:1403–12. http://dx.doi.org/10.1093/infdis/jir525

8. Zhang Z, Zheng Z, Luo H, Meng J, Li H, Li Q, et al. Human bocavirus NP1 inhibits IFN-beta production by blocking association of IFN regulatory factor 3 with IFNB promoter. J Immunol. 2012;189:1144–53. http://dx.doi.org/10.4049/jimmunol.1200096

9. Dupuis M, Hull R, Wang H, Nattanmai S, Glasheen B, Fusco H, et al. Molecular detection of viral causes of encephalitis and meningitis in New York State. J Med Virol. 2011;83:2172–81. http://dx.doi.org/10.1002/jmv.22169

10. Gable MS, Sheriff H, Dalmau J, Tilley DH, Glaser CA. The frequency of autoimmune N-methyl-D-aspartate receptor encephalitis surpasses that of individual viral etiologies in young individuals enrolled in the California Encephalitis Project. Clin Infect Dis. 2012;54:899–904. http://dx.doi.org/10.1093/cid/cir1038

11. Dalmau J, Lancaster E, Martinez-Hernandez E, Rosenfeld MR, Balice-Gordon R. Clinical experience and laboratory investigations in patients with anti-NMDAR encephalitis. Lancet Neurol. 2011;10:63–74. http://dx.doi.org/10.1016/S1474-4422(10)70253-2

12. Soares CN, Cabral-Castro MJ, Peralta JM, de Freitas MR, Zalis M, Puccioni-Sohler M. Review of the etiologies of viral meningitis and encephalitis in a dengue endemic region. J Neurol Sci. 2011;303:75–9. http://dx.doi.org/10.1016/j.jns.2011.01.012

13. Tavakoli NP, Wang H, Nattanmai S, Dupuis M, Fusco H, Hull R. Detection and typing of enteroviruses from CSF specimens from patients diagnosed with meningitis/encephalitis. J Clin Virol. 2008;43:207–11. http://dx.doi.org/10.1016/j.jcv.2008.06.016

14. Frange P, Peffault de Latour R, Arnaud C, Boddaert N, Oualha M, Avettand-Fenoel V, et al. Adenoviral infection presenting as an isolated central nervous system disease without detectable viremia in two children after stem cell transplantation. J Clin Microbiol. 2011;49:2361–4. http://dx.doi.org/10.1128/JCM.00080-11

15. Straussberg R, Harel L, Levy Y, Amir J. A syndrome of transient encephalopathy associated with adenovirus infection. Pediatrics. 2001;107:E69. http://dx.doi.org/10.1542/peds.107.5.e69

Address for correspondence: Kamruddin Ahmed, Research Promotion Institute, Oita University, Yufu 879-5593, Oita, Japan; email: ahmed@oita-u.ac.jp

EMERGING
INFECTIOUS DISEASES*

SUBMIT MANUSCRIPTS - HTTP://MC.MANUSCRIPTCENTRAL.COM/EID/

http://www.cdc.gov/ncidod/eid/instruct.htm

– 160 –

Contents lists available at SciVerse ScienceDirect

Neurochemistry International

Decreased levels of free D-aspartic acid in the forebrain of serine racemase (Srr) knock-out mice

Mao Horio [a,1], Tamaki Ishima [a,1], Yuko Fujita [a], Ran Inoue [b], Hisashi Mori [b], Kenji Hashimoto [a,*]

[a] Division of Clinical Neuroscience, Chiba University Center for Forensic Mental Health, Chiba, Japan
[b] Department of Molecular Neuroscience, Graduate School of Medicine and Pharmaceutical Sciences, University of Toyama, Toyama, Japan

ARTICLE INFO

ABSTRACT

D-Serine, an endogenous co-agonist of the N-methyl-D-aspartate (NMDA) receptor is synthesized from L-serine by serine racemase (SRR). A previous study of Srr knockout (Srr-KO) mice showed that levels of D-serine in forebrain regions, such as frontal cortex, hippocampus, and striatum, but not cerebellum, of mutant mice are significantly lower than those of wild-type (WT) mice, suggesting that SRR is responsible for D-serine production in the forebrain. In this study, we attempted to determine whether SRR affects the level of other amino acids in brain tissue. We found that tissue levels of D-aspartic acid in the forebrains (frontal cortex, hippocampus and striatum) of Srr-KO mice were significantly lower than in WT mice, whereas levels of D-aspartic acid in the cerebellum were not altered. Levels of D-alanine, L-alanine, L-aspartic acid, taurine, asparagine, arginine, threonine, γ-amino butyric acid (GABA) and methionine, remained the same in frontal cortex, hippocampus, striatum and cerebellum of WT and mutant mice. Furthermore, no differences in D-aspartate oxidase (DDO) activity were detected in the forebrains of WT and Srr-KO mice. These results suggest that SRR and/or D-serine may be involved in the production of D-aspartic acid in mouse forebrains, although further detailed studies will be necessary to confirm this finding.
© 2013 Elsevier Ltd. All rights reserved.

1. Introduction

It was a long held belief that only the L-isomers of amino acids existed in mammals. However, with recent advances in analytical methods, free D-amino acids, including D-aspartic acid and D-serine, have been found in the tissues of mammals, including humans (Dunlop et al., 1986; Hashimoto et al., 1992; Nagata, 1992; Nagata et al., 1992a,b; Brückner and Hausch, 1993). Subsequent studies using two-dimensional high performance liquid chromatography (HPLC), detected very low levels of free D-amino acids in a variety of mammalian tissues (Hamase et al., 2001, 2005; Morikawa et al., 2001; Miyoshi et al., 2009, 2012; Yamanaka et al., 2012). It is therefore not unreasonable to conclude that D-amino acids may play a role in physiological and biological functions in mammals. Of the free D-amino acids, the roles of D-aspartic acid, D-serine and D-alanine have been well investigated in animal brains (Hashimoto and Oka, 1997; Hamase, 2007; Yamanaka et al., 2012).

D-Serine, an endogenous co-agonist of the N-methyl-D-aspartate (NMDA) receptor, plays an important role in excitatory neurotransmission, via the NMDA receptor (Hashimoto et al., 1993; Schell

et al., 1997). D-Serine is synthesized from L-serine by the pyridoxal-5′ phosphate-dependent enzyme, serine racemase (SRR) (Wolosker et al., 1999a, b), and metabolized by D-amino acid oxidase (DAAO) (Wolosker and Mori, 2012). Studies using Srr knockout (Srr-KO) mice have shown that SRR is predominantly localized to forebrain neurons (Miya et al., 2008) and that levels of D-serine in the forebrain of these animals are 80–90% lower than in wild-type (WT) mice (Inoue et al., 2008; Basu et al., 2009; Horio et al., 2011), implying that D-serine production in the forebrain is largely dependent on SRR activity. In contrast, levels of L-serine, glycine, glutamine and glutamate, which are also related to NMDA receptor neurotransmission, were similar between brain tissue from Srr-KO and WT mice (Horio et al., 2011).

D-Aspartic acid was the first D-amino acid found in mammalian brains (Dunlop et al., 1986) and it is observed in many neuroendocrine and endocrine organs (Hashimoto et al., 1995). It is directly involved in the secretion of hormones, such as melatonin and testosterone (D'Aniello et al., 1996; Takigawa et al., 1998; Huang et al., 2006). D-Aspartic acid is synthesized by the pyridoxal-5′ phosphate-dependent enzyme, aspartate racemase in adult mouse brain (Kim et al., 2010), and degraded by D-aspartate oxidase (DDO) (Van Veldhoven et al., 1991; Huang et al., 2006). Due to its structural similarity to NMDA, D-aspartic acid binds to the NMDA receptor and potentiates NMDA receptor-mediated neurotransmission (Fagg and Matus, 1984; D'Aniello et al., 2011; Yamanaka et al., 2012). Like D-serine, D-alanine is also an

endogenous co-agonist of the NMDA receptor although its synthetic pathway is unknown (Kleckner and Dingledine, 1988; McBrain et al., 1989). Interestingly, increased levels of D-alanine in brain tissue and plasma were observed in patients with Alzheimer's (Fisher et al., 1991) and renal diseases (Nagata et al., 1992a).

In this study, we measured levels of D-aspartic acid and D-alanine, as well as the amino acids, L-alanine, L-aspartate, taurine, asparagine, arginine, threonine, γ-amino butyric acid (GABA) and methionine, from frontal cortex, hippocampus, striatum and cerebellum of wild-type (WT) and Srr-KO mice. Additionally, we measured the activity of DDO in the forebrain of WT and Srr-KO mice.

2. Materials and methods

2.1. Animals

The Srr-KO mice were generated from C57BL/6- derived embryonic stem cells transfected with a gene-targeting vector containing C57BL/6 mouse genomic DNA, and the colony expanded by crossing with C57BL/6 mice (Miya et al., 2008). The generation and genotyping of Srr-KO mice and wild-type (WT) control mice with a pure C57BL/6 genetic background has been reported previously (Miya et al., 2008). WT and Srr-KO male mice aged 2–3 months were used for analyses. The mice were housed in clear polycarbonate cages (22.5 × 33.8 × 14.0 cm) in groups of 5 or 6 per cage under a controlled 12/12-h light–dark cycle (lights on from 7:00a.m. to 7:00p.m.), with a room temperature of 23 ± 1 °C and humidity of 55 ± 5%. The mice were given free access to water and food pellets. Experimental procedures were approved by the Animal Care and Use Committee of Chiba University.

2.2. Sample preparation

Twenty-four hours after fasting, mice were sacrificed by decapitation. Then, brain regions, the frontal cortex, hippocampus, striatum, and cerebellum were dissected on ice. All samples were stored at −80 °C before analysis.

2.3. HPLC system for the determination of D- and L-aspartic acid, and D- and L-alanine

Tissues were homogenized in 1.5 mL of methanol (HPLC grade) on ice. The homogenates were centrifuged at 3000g for 6 min at 4 °C, and 20 μL of supernatant was evaporated to dryness at 40 °C. To the residue, 20 μL of H_2O (HPLC grade), 20 μL of 0.1 M borate buffer (pH 8.0) and 60 μL of 50 mM 4-fluoro-7-nitro-2,1,3-benzoxadiazole (NBD-F; Tokyo Kasei Kogyo Co., Ltd., Tokyo, Japan) in CH_3CN (HPLC grade) were added. The reaction mixture was then heated to 60 °C for 2 min, and immediately supplemented with 100 μL of H_2O/acteonitrile (92/8) containing 0.05% trifluoroacetic acid to stop the reaction. These procedures were fully automated using a 3023 auto sampler.

Measurement of D- and L-aspartic acid, and D- and L-alanine was performed using the previous reports with a slight modification (Morikawa et al., 2001; Miyoshi et al., 2009, 2012). The HPLC system (NANOSPACE SI-2 series, Shiseido Ltd, Tokyo, Japan) consisted of a type 3202 degasser, 3101 and 3201 pumps, a 3023 auto sampler, 3004 and 3014 column oven, two 3213 fluorescence detectors, a 3011 column-switching high pressure valve and dual-loop valve. A data processing programs, EzChrom Elite Client, was used to monitor the detectors response and a column-switching valve and a dual-loop valve were controlled by a KSAA valve controlling system (Shiseido Ltd, Tokyo, Japan).

The analytical column for the reversed-phase separation was a Nucleonavi (250 mm × 1.0 mm i.d., Shiseido Ltd., Tokyo, Japan)

maintained at 40 °C. Mobile phase 1a consisted of H_2O/acetonitrile (92/8) containing 0.05% TFA, and phases 1b, H_2O/acetonitrile (10/90) containing 0.1% TFA and acetonitrile, respectively. The gradient elution of the mobile phase was kept at a constant flow rate of 50 μL/min. The time program for gradient elution was as follows: 0–40.0 min 1a: 1b = 100: 0, 40.0–40.1 min liner gradient from 0% 1b to 100% 1b,40.1–50.0 min 1a: 1b = 0: 100, 50.0–50.1 min liner gradient from 0% 1a to 100% 1a, and 50.1–120 min 1a: 1b = 100: 0. The chiral column (Column 2) used for the separation and quantification of D- and L-aspartic acid, and D- and L-alanine with NBD-F comprised two KSAA-OA2500 columns (S) (250 mm × 2.0 mm i.d., Shiseido Ltd., Tokyo, Japan), which were connected in tandem. The mobile phase was 15 mM citric acid in methanol. The flow rate was isocratically pumped at 200 μL/min. The column temperature was maintained at 25 °C for all columns. Fluorescence detection was performed at 530 nm with an excitation wavelength at 470 nm.

2.4. HPLC system for the determination of various amino acids

Measurements of taurine, asparagine, arginine, threonine, γ-amino butyric acid (GABA) and methionine were carried out using a HPLC system with fluorescence detection, as previously reported (Aoyama et al., 2004). Tissues were homogenized in 1.5 mL of methanol (HPLC grade) on ice. The homogenates were centrifuged at 3000g for 6 min at 4 °C, and 20 μL of supernatant was evaporated to dryness at 40 °C. To the residue, 25 μL of H_2O (HPLC grade), 20 μL of internal standard solution (375 nM ε-amino-n-caproic acid in water), 25 μL of 0.2 M borate buffer (pH 9.5) and 30 μL of 10 mM NBD-F (Tokyo Kasei Kogyo Co., Ltd., Tokyo, Japan) in CH_3CN (HPLC grade) were added. The reaction mixture was put at room temperature for 40 min, and immediately supplemented with 50 μL of 1 M tartrate buffer (pH 2.0) to stop the reaction. These procedures were fully automated using a SIL-20A auto sampler.

The HPLC system (SCL-10A vp series, Shimadzu Ltd., Tokyo, Japan) consisted of a type DGU-20A₅ degasser, a LC-20A pumps, a SIL-20AC auto sampler, a CTO-20A column oven, a RF-10A$_{XL}$ fluorescence detectors, for the determination of taurine, asparagine, arginine, threonine, GABA and methionine, a cadenza CD-C18 ODS column (250 mm × 4.6 mm i.d., Imtakt, Ltd., Kyoto, Japan) was used. The gradient elution of the mobile phase was kept at a constant flow rate of 0.8 mL/min. Mobile phase A consisted of H_2O/acetonitrile/2-propanol (90/10/0.8) containing 0.08% TFA, and phases B, C and D, of H_2O/acetonitrile/2-propanol (90/10/5) containing 0.08% TFA, H_2O/acetonitrile (90/10) and H_2O/acetonitrile (10/90) containing 0.08% TFA acetonitrile, respectively.

The time program for gradient elution was programmed as follows: 0–25 min A: B: C: D = 100: 0: 0: 0, 25–32 min liner gradient from 0% B to 100% B, 32–35 min A: B: C: D = 0: 100: 0: 0, 35–39 min liner gradient from 100% B to 97% B, 39–45 min A: B: C: D = 0: 97: 0: 3, 45–45.1 min liner gradient from 97% B to 0% B, 45.1–60 min A: B: C: D = 0: 0: 90: 10, 60–60.1 min liner gradient from 90% C to 65% C, 60.1–63 min A: B: C: D = 0: 0: 65: 35, 63–63.1 min liner gradient from 0% B to 15% B, 63.1–68 min A: B: C: D = 0: 15: 55: 30, 68–70 min liner gradient from 55% C to 50% C, 70–82 min A: B: C: D = 0: 15: 50: 35, 82–85 min liner gradient from 15% B to 0% B, 85.1–100 min A: B: C: D = 0: 0: 40: 60, 100–100.1 min liner gradient from 0% A to 100% A and 100–120 min, A: B: C: D = 100: 0: 0: 0. Injection volume was 20 μL. All column temperatures were maintained at 35 °C. Fluorescence detection was performed at 530 nm with an excitation wavelength at 470 nm.

2.5. Measurement of DDO activity

The activity of DDO in the forebrain and kidney (a high DDO activity tissue) was measured as previously reported (Yamada et al., 1988; D'Aniello et al., 1993). Briefly, tissue was homogenized

with 4-volumes of 50 mM Tris–HCl (pH 8.2) at 4 °C, and centri-fuged at 30,000g for 30 min. Then, the supernatant was incubated with 20 µM FAD (flavin adenine dinucleotide) 100 mM D-aspartic acid (pH 8.3, adjusted with NaOH), to a final volume of 0.5 mL. The mixture was incubated at 37 °C with shaking, for 30 min. After the addition of 0.2 mL of 25% trichloroacetic acid and centrifuga-tion, 0.2 mL of supernatant was mixed with 0.1 mL of 0.1% 2,4-dini-trophenylhydrazine in 2 M HCl, and incubated for 10 min at 37 °C. A 0.2 mL aliquot of 3.75 M NaOH was then added to the solution and it was left to stand for 10 min. Supernatant absorbance was measured at 445 nm, where 2,4-dinitrophenylhydrazones of oxalo-acetate and pyruvate showed approximately the same molar absorption coefficient. Samples were measured against a blank ref-erence prepared using the reaction mixture without D-aspartic acid. The assays were performed in duplicate.

2.6. Statistical analysis

The data are presented as the mean ± standard error of the mean (S.E.M.). Statistical analysis was performed using Student's t-test. The p values less than 0.05 were considered statistically significant.

3. Result

3.1. Levels of D-aspartic acid and D-alanine in brain tissue

Tissue levels of D- and L-aspartic acid and D- and L-alanine in the frontal cortex, hippocampus, striatum and cerebellum of WT and Srr-KO mice are shown in Table 1. Levels of D-aspartic acid in the frontal cortex ($t = 3.209$, $p = 0.005$), hippocampus ($t = 7.403$, $p < 0.001$) and striatum ($t = 5.051$, $p < 0.001$) of Srr-KO mice were significantly lower than those of WT mice (Fig. 1 and Table 1). However, in the cerebellum, where levels of D-aspartic acid are nat-urally markedly lower than the frontal cortex, hippocampus, and striatum, there was no difference between Srr-KO and WT mice (Fig. 1 and Table 1). Brain tissue levels of L-aspartic acid, D-alanine and L-alanine were comparable between Srr-KO and WT mice (Table 1).

3.2. Levels of selected amino acids in brain tissue

Tissue levels of taurine, asparagine, arginine, threonine, GABA and methionine in the brains of WT and Srr-KO mice are shown in Table 2. Levels of these amino acids in the frontal cortex, hippo-campus, striatum and cerebellum of Srr-KO mice were comparable to levels in WT mice (Table 2).
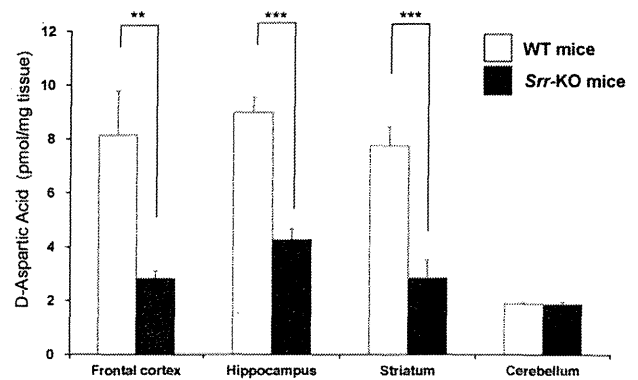

Fig. 1. Levels of D-aspartic acid in the frontal cortex, hippocampus, striatum, and cerebellum. Levels of D-aspartic acid in the frontal cortex, hippocampus, and striatum of Srr-KO mice were significantly lower than in WT mice. In contrast, levels of D-aspartic acid in the cerebellum of Srr-KO mice were not different from WT mice. This data shows the mean ± SEM (n = 10). **$p < 0.01$, ***$p < 0.001$ when compared to WT mice.

3.3. DDO activity in the forebrain and kidney

We measured the activity of DDO in the forebrain of mice, to determine the effects of its activity on D-aspartic acid levels. We also measured DDO activity in the kidney, since this tissue typi-cally shows high activity (Yamada et al., 1988; D'Aniello et al., 1993). DDO activity in the forebrain was greatly lower than that in the kidney, consistent with previous data (Yamada et al., 1988) (Table 3). There were no differences ($t = -0.760$, $p = 0.461$) in DDO activity in the forebrains of WT and Srr-KO mice (Table 3). However, we found that DDO activity in the kidney was signifi-cantly lower in Srr-KO mice ($t = 5.117$, $p < 0.001$), relative to WT mice (Table 3). In addition, the weight of kidneys from Srr-KO mice was also significantly ($t = 5.690$, $p < 0.001$) lower than those of WT mice (Table 3).

4. Discussion

This study found that levels of free D-aspartic acid in the fore-brain of Srr-KO mice were significantly lower than those of WT mice, although levels of other amino acids were similar between Srr-KO and WT mouse brains. Forebrain regions such as, frontal cortex, hippocampus, and striatum, show high density expression of SRR and D-serine, whereas the cerebellum shows very low expression (Miya et al., 2008; Horio et al., 2011). Previously, we re-ported that SRR is the enzyme most likely responsible for D-serine production in mouse forebrains, as Srr-KO mice show an 80–90%

Table 1
Tissue levels of D- and L-aspartic acid, and D- and L-alanine in mouse brains.

Brain region	Genotype	pmol/mg tissue		nmol/mg tissue	
		D-Aspartic acid	D-Alanine	L-Aspartic acid	L-Alanine
Frontal cortex	WT	8.15 ± 1.64	1.51 ± 0.16	0.59 ± 0.13	0.42 ± 0.03
	Srr-KO	2.82 ± 0.27**	1.39 ± 0.11	0.44 ± 0.02	0.37 ± 0.02
Hippocampus	WT	9.00 ± 0.55	0.81 ± 0.10	0.66 ± 0.04	0.27 ± 0.03
	Srr-KO	4.27 ± 0.41***	0.74 ± 0.24	0.66 ± 0.04	0.25 ± 0.02
Striatum	WT	7.77 ± 0.69	0.37 ± 0.10	0.39 ± 0.02	0.10 ± 0.02
	Srr-KO	2.85 ± 0.69***	0.26 ± 0.04	0.39 ± 0.02	0.10 ± 0.01
Cerebellum	WT	1.89 ± 0.05	0.40 ± 0.06	0.54 ± 0.04	0.20 ± 0.01
	Srr-KO	1.86 ± 0.08	0.31 ± 0.02	0.55 ± 0.02	0.19 ± 0.01

Values are the mean ± SEM (n = 10).
** $p < 0.01$.
*** $p < 0.001$ compared with WT mice.

Table 2
Tissue levels of amino acids in mouse brains.

Regions	Genotype	Taurine	Aspargine	Arginine	Threonine	GABA	Methionine
Frontal cortex	WT	464.8 ± 17.8	5.9 ± 1.3	164.7 ± 26.1	1152.1 ± 252.6	190.8 ± 24.4	68.3 ± 1.9
	Srr-KO	436.7 ± 5.5	7.5 ± 0.6	128.1 ± 22.2	332.5 ± 114.1	182.7 ± 18.8	75.0 ± 3.5
Hippocampus	WT	382.3 ± 15.9	10.6 ± 0.6	3.0 ± 0.2	72.8 ± 30.0	199.9 ± 21.8	71.8 ± 4.3
	Srr-KO	328.6 ± 7.2	8.4 ± 0.2	2.4 ± 0.1	60.0 ± 21.2	164.8 ± 18.6	60.0 ± 3.4
Striatum	WT	438.3 ± 27.9	25.8 ± 4.7	87.0 ± 10.1	120.0 ± 35.4	256.8 ± 39.0	68.9 ± 5.8
	Srr-KO	370.2 ± 11.9	19.2 ± 2.6	85.0 ± 6.1	133.8 ± 41.3	213.1 ± 30.2	48.9 ± 4.8
Cerebellum	WT	338.0 ± 15.0	8.1 ± 0.4	383.4 ± 16.1	78.8 ± 18.3	153.1 ± 25.1	14.7 ± 2.7
	Srr-KO	299.3 ± 6.4	7.3 ± 0.2	351.7 ± 10.4	74.7 ± 16.4	131.8 ± 21.2	7.1 ± 0.3

Values (pmol/mg tissue) are the mean ± SEM (n = 10).

Table 3
DDO activity in the forebrain and kidney of WT and Srr-KO mice.

Tissues	DDO activity (nmol/g tissue/min)	
	WT	Srr-KO
Forebrain	3.15 ± 0.58	3.82 ± 0.64
Kidney	99.43 ± 3.73	60.26 ± 6.68[***]
Weight (mg)	310.7 ± 4.32	256.2 ± 8.55[***]

Values are the mean ± SEM (n = 7 or 8).
[***] $p < 0.001$ as compared with WT mice (Student's t-test).

decrease in this amino acid, within the frontal cortex, hippocampus and striatum (Horio et al., 2011). SRR is highly selective for L-serine relative to other amino acids. Substrate specificity of L-alanine and L-aspartate were 1.5% and 0% of control values (100% for L-serine), respectively (Wolosker et al., 1999b), indicating that SRR does not play a role in the direct production of D-aspartic acid from L-aspartic acid. In this study, we found that cerebellum levels of D-aspartic acid and D-serine were unaltered between Srr-KO and WT mice (Horio et al., 2011). It seems that levels of D-aspartate may be dependent upon D-serine levels in the forebrain, although this needs further examination.

High levels of D-aspartic acid are readily detectable in peripheral organs, including adrenal, testis, and spleen (Hashimoto et al., 1993; Hashimoto and Oka, 1997; D'Aniello et al., 1996; Han et al., 2011). In this study, we found that levels of D-aspartic acid in the testis of Srr-KO mice were no different to those of WT mice (Supplemental Fig. 1). It seems likely then, that decreased levels of D-aspartic acid in the forebrain of Srr-KO mice is a forebrain-specific effect, although this needs to be tested.

D-Aspartic acid is synthesized from L-aspartic acid by aspartate racemase (Kim et al., 2010). Depletion of aspartate racemase by retroviral-mediated expression of short-hairpin RNA, highlighted an important role for this enzyme in neuronal development, and is consistent with the high levels of D-aspartic acid noted during early neuronal ontogeny (Kim et al., 2010). A study analyzing DDO-deficient (DDO$^{-/-}$) mice found increased levels of D-aspartic acid in the brains of these mice, suggesting that D-aspartic acid is an endogenous substrate of DDO (Huang et al., 2006). Previous reports found high DDO activity in the kidneys of mice and rats (Yamada et al., 1988; D'Aniello et al., 1993). In this study, we found no difference in forebrain DDO activity between WT and Srr-KO mice, suggesting that DDO may not play a role in the reduced levels of D-aspartic acid seen in the forebrain of Srr-KO mice. The precise reasons underlying the reduced levels of D-aspartic acid in the forebrain of Srr-KO mice are currently unknown. One possibility is that SRR and/or D-serine could affect the activity of aspartate racemase in the forebrain. Another possibility is that D-aspartic acid may be synthesized from D-serine via unknown pathways. Nonetheless, further detailed studies on the relationship between D-aspartic acid and SRR/D-serine signaling are needed.

In this study, we found that DDO activity in the kidneys of Srr-KO mice was significantly lower than that of WT mice. We also found that kidneys from Srr-KO mice were significantly lower in weight compared to kidneys from WT mice. The precise reasons underlying reduced DDO activity levels in the kidney of Srr-KO mice are currently unknown. Considering our findings, it seems that Srr-KO mice may suffer impaired kidney function, although further studies are necessary to confirm this point.

5. Conclusion

This study showed that forebrain tissue levels of D-aspartic acid from Srr-KO mice were significantly lower than those of WT mice, although other amino acid levels remained unchanged. These results suggest that SRR and/or D-serine may be involved in the production of D-aspartic acid in mouse forebrain, although further detailed studies are required to support this finding.

Appendix A. Supplementary data

Supplementary data associated with this article can be found, in the online version, at http://dx.doi.org/10.1016/j.neuint.2013.02.015.

References

Aoyama, C., Santa, T., Tsunoda, M., Fukushima, T., Kitada, C., Imai, K., 2004. A fully automated amino acid analyzer using NBD-F as a fluorescent derivatization reagent. Biomed. Chromatogr. 18, 630–636.

Basu, A.C., Tsai, G.E., Ma, C.L., Ehmsen, J.T., Mustafa, A.K., Han, L., Jiang, Z.I., Benneyworth, M.A., Froimowitz, M.P., Lange, N., Snyder, S.H., Bergeron, R., Coyle, J.T., 2009. Targeted disruption of serine racemase affects glutamatergic neurotransmission and behavior. Mol. Psychiatry. 14, 719–727.

Brückner, H., Hausch, M., 1993. Gas chromatographic characterization of free D-amino acids in the blood serum of patients with renal disorders and of healthy volunteers. J. Chromatogr. 614, 7–17.

D'Aniello, A., Di Cosmo, A., Di Cristo, C., Annunziato, L., Petrucelli, L., Fisher, G., 1996. Involvement of D-aspartic acid in the synthesis of testosterone in rat testes. Life Sci. 59, 97–104.

D'Aniello, A., D'Onofrio, G., Pischetola, M., D'Aniello, G., Vetere, A., Petrucelli, L., Fisher, G.H., 1993. Biological role of D-amino acid oxidase and D-aspartate oxidase. Effects of D-amino acids. J. Biol. Chem. 268, 26941–26949.

D'Aniello, S., Somorjai, I., Garcia-Fernàndez, J., Topo, E., D'Aniello, A., 2011. D-Aspartic acid is a novel endogenous neurotransmitter. FASEB J. 25, 1014–1027.

Dunlop, D.S., Neidle, A., McHale, D., Dunlop, D.M., Lajtha, A., 1986. The presence of free D-aspartic acid in rodents and man. Biochem. Biophys. Res. Commun. 141, 27–32.

Fagg, G.E., Matus, A., 1984. Selective association of N-methyl aspartate and quisqualate types of L-glutamate receptor with brain postsynaptic densities. Proc. Natl. Acad. Sci. USA 81, 6876–6880.

Fisher, G.H., D'Aniello, A., Vetere, A., Padula, L., Cusano, G.P., Man, E.H., 1991. Free D-aspartate and D-alanine in normal and Alzheimer brain. Brain Res. Bull. 26, 983–985.

Hamase, K., 2007. Sensitive two-dimensional determination of small amounts of D-amino acids in mammals and the study on their functions. Chem. Pharm. Bull. (Tokyo) 55, 503–510.

Hamase, K., Konno, R., Morikawa, A., Zaitsu, K., 2005. Sensitive determination of D-amino acids in mammals and the effect of D-amino-acid oxidase activity on their amounts. Biol. Pharm. Bull. 28, 1578–1584.

Hamase, K., Inoue, T., Morikawa, A., Konno, R., Zaitsu, K., 2001. Determination of free D-proline and D-leucine in the brains of mutant mice lacking D-amino acid oxidase activity. Anal. Biochem. 298, 253–258.

Han, H., Miyoshi, Y., Ueno, K., Okamura, C., Tojo, Y., Mita, M., Lindner, W., Zaitsu, K., Hamase, K., 2011. Simultaneous determination of D-aspartic acid and D-glutamic acid in rat tissues and physiological fluids using a multi-loop two-dimensional HPLC procedure. J. Chromatogr. B Analyt. Technol. Biomed. Life Sci. 879, 3196–3202.

Hashimoto, A., Nishikawa, T., Oka, T., Takahashi, K., 1993a. Endogenous D-serine in rat brain: N-methyl-D-aspartate receptor-related distribution and aging. J. Neurochem. 60, 783–786.

Hashimoto, A., Nishikawa, T., Oka, T., Hayashi, T., Takahashi, K., 1993b. Widespread distribution of free D-aspartate in rat periphery. FEBS Lett. 331, 4–8.

Hashimoto, A., Nishikawa, T., Oka, T., Takahashi, K., Hayashi, T., 1992. Determination of free amino acid enantiomers in rat brain and serum by high-performance liquid chromatography after derivatization with N-tert-butyloxycarbonyl-L-cysteine and o-phthaldialdehyde. J. Chromatogr. 582, 41–48.

Hashimoto, A., Oka, T., 1997. Free D-aspartate and D-serine in the mammalian brain and periphery. Prog. Neurobiol. 52, 325–353.

Hashimoto, A., Oka, T., Nishikawa, T., 1995. Anatomical distribution and postnatal changes in endogenous free D-aspartate and D-serine in rat brain and periphery. Eur. J. Neurosci. 7, 1657–1663.

Horio, M., Kohno, M., Fujita, Y., Ishima, T., Inoue, R., Mori, H., Hashimoto, K., 2011. Levels of D-serine in the brain and peripheral organs of serine racemase (Srr) knock-out mice. Neurochem. Int. 59, 853–859.

Huang, A.S., Beigneux, A., Weil, Z.M., Kim, P.M., Molliver, M.E., Blackshaw, S., Nelson, R.J., Young, S.G., Snyder, S.H., 2006. D-aspartate regulates melanocortin formation and function: behavioral alterations in D-aspartate oxidase-deficient mice. J. Neurosci. 26, 2814–2819.

Inoue, R., Hashimoto, K., Harai, T., Mori, H., 2008. NMDA- and beta-amyloid$_{1-42}$-induced neurotoxicity is attenuated in serine racemase knock-out mice. J. Neurosci. 28, 14486–14491.

Kim, P.M., Duan, X., Huang, A.S., Liu, C.Y., Ming, G.L., Song, H., Snyder, S.H., 2010. Aspartate racemase, generating neuronal D-aspartate, regulates adult neurogenesis. Proc. Natl. Acad. Sci. USA 107, 3175–3179.

Kleckner, N.W., Dingledine, R., 1988. Requirement for glycine in activation of NMDA-receptors expressed in Xenopus oocytes. Science 241, 835–837.

McBrain, C.J., Kleckner, N.W., Wyrick, S., Dingledine, R., 1989. Structural requirements for activation of the glycine coagonist site of N-methyl-D-

aspartate receptors expressed in Xenopus oocytes. Mol. Pharmacol. 36, 556–565.

Miya, K., Inoue, R., Takata, Y., Abe, M., Natsume, R., Sakimura, K., Hongou, K., Miyawaki, T., Mori, H., 2008. Serine racemase is predominantly localized in neurons in mouse brain. J. Comp. Neurol. 510, 641–654.

Miyoshi, Y., Hamase, K., Tojo, Y., Mita, M., Konno, R., Zaitsu, K., 2009. Determination of D-serine and D-alanine in the tissues and physiological fluids of mice with various D-amino-acid oxidase activities using two-dimensional high-performance liquid chromatography with fluorescence detection. J. Chromatogr. B Analyt. Techol. Biomed. Life Sci. 877, 2506–2512.

Miyoshi, Y., Koga, R., Oyama, T., Han, H., Ueno, K., Masuyama, K., Itoh, Y., Hamase, K., 2012. HPLC analysis of naturally occurring free D-amino acids in mammals. J. Pharm. Biomed. Anal. 69, 42–49.

Morikawa, A., Hamase, K., Inoue, T., Konno, R., Niwa, A., Zaitsu, K., 2001. Determination of free D-aspartic acid, D-serine and D-alanine in the brain of mutant mice lacking D-amino acid oxidase activity. J. Chromatogr. B Biomed. Sci. Appl. 757, 119–125.

Nagata, Y., 1992. Involvement of D-amino acid oxidase in elimination of D-serine in mouse brain. Experientia 48, 753–755.

Nagata, Y., Masui, R., Akino, T., 1992a. The presence of free D-serine, D-alanine and D-proline in human plasma. Experientia 48, 986–988.

Nagata, Y., Yamamoto, K., Shimojo, T., Konno, R., Yasumura, Y., Akino, T., 1992b. The presence of free D-alanine, D-proline and D-serine in mice. Biochim. Biophys. Acta 1115, 208–211.

Schell, M.J., Brady Jr., R.O., Molliver, M.E., Snyder, S.H., 1997. D-Serine as a neuromodulator: regional and developmental localizations in rat brain glia resemble NMDA receptors. J. Neurosci. 17, 1604–1615.

Takigawa, Y., Homma, H., Lee, J.A., Fukushima, T., Santa, T., Iwatsubo, T., Imai, K., 1998. D-aspartate uptake into cultured rat pinealocytes and the concomitant effect on L-aspartate levels and melatonin secretion. Biochem. Biophys. Res. Commun. 248, 641–647.

Van Veldhoven, P.P., Brees, C., Mannaerts, G.P., 1991. D-Aspartate oxidase, a peroxisomal enzyme in liver of rat and man. Biochim. Biophys. Acta 1073, 203–208.

Wolosker, H., Blackshaw, S., Snyder, S.H., 1999a. Serine racemase: a glial enzyme synthesizing D-serine to regulate glutamate-N-methyl-D-aspartate neurotransmission. Proc. Natl. Acad. Sci. USA 96, 13409–13414.

Wolosker, H., Sheth, K.N., Takahashi, M., Mothet, J.P., Brady, R.O., Ferris, C.D., Snyder, S.H., 1999b. Purification of serine racemase: biosynthesis of the neuromodulator D-serine. Proc. Natl. Acad. Sci. USA 96, 721–725.

Wolosker, H., Mori, H., 2012. Serine racemase: an unconventional enzyme for an unconventional transmitter. Amino Acids 43, 1895–1904.

Yamada, R., Nagasaki, H., Wakabayashi, Y., Iwashima, A., 1988. Presence of D-aspartate oxidase in rat liver and mouse tissues. Biochem. Biophys. Acta 965, 202–205.

Yamanaka, M., Miyoshi, Y., Ohide, H., Hamase, K., Konno, R., 2012. D-Amino acids in the brain and mutant rodents lacking D-amino acid oxidase activity. Amino acids 43, 1811–1821.

CORRESPONDENCE

Is D-Cycloserine a Prodrug for D-Serine in the Brain?

To the Editor:

D-cycloserine (DCS), (4R)-4-amino-1,2-oxazolidin-3-one, is a partial agonist at the strychnine-insensitive glycine modulatory site associated with the N-methyl-D-aspartate (NMDA) receptor complex. DCS is also a less efficient ligand of NMDA receptor function than endogenous full agonists, such as glycine and D-serine. At high doses, DCS acts as an antagonist by displacing more efficacious endogenous agonists, but at moderate doses, DCS facilitates glutamatergic neurotransmission via the NMDA receptor. Recent meta-analysis shows that glycine, D-serine, and sarcosine (N-methylglycine), an endogenous glycine transporter-1 inhibitor, are more effective than DCS in improving the overall psychopathology in patients with schizophrenia receiving antipsychotic drugs (1). This suggests a relatively narrow therapeutic window for DCS, most likely due to its partial agonist properties.

A meta-analysis of both animals and humans demonstrated that DCS enhances prolonged exposure therapy, a cognitive-behavioral therapy, used in patients with anxiety disorders, such as posttraumatic stress disorder (PTSD), social phobia, panic disorder, and obsessive-compulsive disorder (2), although a recent meta-analysis conducted in humans showed no significant effects of dose timing or dose number on the treatment efficacy of DCS (3). Animal studies have suggested that fear of extinction has been linked to NMDA receptor function in the basolateral amygdala and that DCS can enhance extinction effects (4). When fear extinction takes place during DCS treatment, the usual forms of neuroplasticity are enhanced, along with the recruitment of additional forms of neuroplasticity, to enhance extinction and protect against reinstatement (5). These findings imply that DCS could be an effective therapeutic agent for enhancing exposure-based therapy in anxiety disorders (2,3,5), although further detailed studies are needed.

Here we report that treatment with DCS can increase extracellular levels of D-serine in the brain. An in vivo microdialysis study using free-moving mice showed that extracellular levels of D-serine in the mouse hippocampus were significantly increased after oral (100 mg/kg) or intracerebroventricular (ICV) infusion of DCS (10 mmol/L, 1 μL/min for 30 min; Figure 1). Previously, we reported that extracellular levels of D-serine in the hippocampus of serine racemase (Srr) knockout (KO) mice were markedly decreased to approximately 20% of levels in wild-type mice, indicating that serine racemase (SRR) is the major enzyme responsible for D-serine production in the mouse forebrain (6) (Figure 1). Interestingly, oral dosing or ICV infusion of DCS induced a marked increase in extracellular D-serine levels within the hippocampus of Srr-KO mice (Figure 1). In contrast, DCS administration did not alter extracellular levels of glycine in this region (data not shown). These findings suggest that SRR does not play a role in the mechanisms that induce increases of D-serine in mouse brains after DCS treatment.

It is well known that DCS is unstable in aqueous solutions, where it is converted into the biologically inactive dimer, 2,5-bis-(aminooxymethyl)-3,6-diketopiperazine (7). Furthermore, DCS can be synthesized from the precursor D-serine. Given that SRR is not required for the production of D-serine in the brain after DCS treatment, D-serine may indeed become available on degradation of DCS because of the inherent instability of DCS in brain extracellular fluids. Interestingly, a pilot study showed that D-serine (30 mg/kg/day) was effective in treating PTSD (8). It is therefore likely that the D-serine produced in the brain after DCS treatment plays at least a partial role in the therapeutic effects of DCS seen in patients with anxiety disorders. Nonetheless, additional study using DCS labeled with isotopes will be needed to confirm this hypothesis.
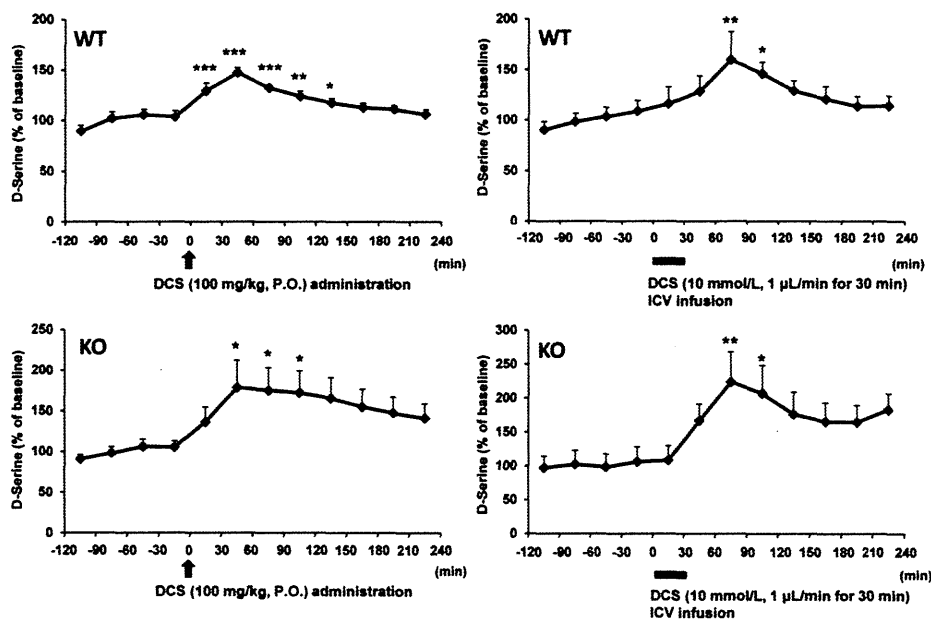

Figure 1. Extracellular D-serine levels in the hippocampus after D-cycloserine (DCS) treatment. Extracellular levels of D-serine in the hippocampus of wild-type (WT) mice and Srr-knockout (KO) mice were significantly increased after oral (P.O.; 100 mg/kg) or intracerebroventricular (ICV; 10 mmol/L, 1 μL/min for 30 min) administration of DCS. The average values of baseline in the hippocampus of WT mice and Srr-KO mice were .358 ± .015 μmol/L (n = 12) and .075 ± .002 μmol/L (n = 12), respectively. Data show the mean ± SEM. Data were analyzed using one-way analysis of variance, post hoc Fisher's protected least significant difference to compare individual postinjection time points to collapsed average baselines values (100%). *p < .05, **p < .01, ***p < .001 compared with baseline values.

Taking all of this information together, it is reasonable to propose that DCS may act as a prodrug for D-serine in the brain. This idea is based on the greater permeability of DCS into the brain compared with D-serine and the unstable nature of DCS in brain extracellular fluids. This degradation of DCS will result in increased D-serine bioavailability within the brain. However, there is also the possibility that the action of D-serine produced from DCS may in turn be antagonized by DCS, resulting in no significant effects in its treatment efficacy for anxiety disorders (3). The low availability of D-serine due to degradation by D-amino acid oxidase in peripheral organs hampers its use in disease treatment because high levels would be needed to achieve therapeutic doses. Therapeutic levels could be achieved if D-serine were administered with D-amino acid oxidase inhibitors. This combination may well provide a more effective and an alternative therapeutic approach to that of DCS (9,10).

Mao Horio[a]

Hisashi Mori[b]

Kenji Hashimoto[a]*

[a]Division of Clinical Neuroscience, Chiba University Center for Forensic Mental Health, Chiba, Japan, and [b]Department of Molecular Neuroscience, Graduate School of Medicine and Pharmaceutical Sciences, University of Toyama, Toyama, Japan
*Corresponding author E-mail: hashimoto@faculty.chiba-u.jp.

1. Tsai GE, Lin PY (2010): Strategies to enhance N-methyl-D-aspartate receptor-mediated neurotransmission in schizophrenia. A critical review and meta-analysis. Curr Pham Des 16:522–537.
2. Nordberg MM, Krystal JH, Tolin DF (2008): A meta-analysis of D-cycloserine and the facilitation of fear extinction and exposure therapy. Biol Psychiatry 63:1118–1126.
3. Bontempo A, Panza KE, Bloch MH (2012): D-Cycloserine augmentation of behavioral therapy for the treatment of anxiety disorders: A meta-analysis. J Clin Psychiatry 73:533–537.
4. Davis M, Ressler K, Rothbaum RO, Richardson R (2006): Effects of D-cycloserine on extinction: Translation from preclinical to clinical work. Biol Psychiatry 60:369–375.
5. Krystal LH (2012): Enhancing prolonged exposure therapy for posttraumatic stress disorder with D-cycloserine: Further support for treatments that promote experience-dependent neuroplasticity. Biol Psychiatry 71:932–934.
6. Horio M, Kohno M, Fujita Y, Ishima T, Inoue R, Mori H, et al. (2011): Levels of D-serine in the brain and peripheral organs of serine racemase (Srr) knock-out mice. Neurochem Int 59:853–859.
7. Higy PH, Hodge EB, Young VV, Harned RL, Brewer GA, Philips WF, et al. (1955): Structure and reactions of cycloserine. J Am Chem Soc 77:2345–2346.
8. Heresco-Levy U, Vass A, Bloch B, Wolosker H, Dumin E, Balan L, et al. (2009): Pilot controlled trial of D-serine for the treatment of post-traumatic stress disorder. Int J Neuropsychopharmacol 12:1275–1282.
9. Ferraris D, Duvall B, Ko YS, Thomas AG, Rojas C, Majer P, et al. (2008) Synthesis and biological evaluation of D-amino acid oxidase inhibitors. J Med Chem 51:3357–3359.
10. Hashimoto K, Fujita Y, Horio M, Kunitachi S, Iyo M, Ferraris D, et al. (2009): Co-administration of D-amino acid oxidase inhibitor potentiates the efficacy of D-serine on prepulse inhibition deficits after administration of dizocilpine. Biol Psychiatry 65:1103–1106.

http://dx.doi.org/10.1016/j.biopsych.2012.07.013

– 167 –

ORIGINAL ARTICLE

Identification and characterization of a novel genetic mutation with prolonged QT syndrome in an unexplained postoperative death

Yukiko Hata · Hisashi Mori · Ayumi Tanaka ·
Yosuke Fujita · Takeshi Shimomura · Toshihide Tabata ·
Koshi Kinoshita · Yoshiaki Yamaguchi · Fukiko Ichida ·
Yoshihiko Kominato · Noriaki Ikeda · Naoki Nishida

Abstract

Introduction The human *ether-à-go-go*-related gene (*hERG*) encodes the α-subunit of a cardiac potassium channel. Various mutations of *hERG*, including missense mutations, have been reported to cause long QT syndrome (LQTS) and severe arrhythmic disorders such as sudden cardiac death. We identified a novel *hERG* frameshift mutation (*hERG*(ΔAT)) in the S5-pore region from a LQTS patient who died suddenly and analyzed its genetic profile and the molecular and electrophysiological behaviors of the protein product to assess the pathogenicity of *hERG*(ΔAT). *Methods and results* We performed direct sequencing of *hERG* and evaluated its transcript level by using a whole blood sample from the patient. We performed immunoblotting, immunocytochemistry, and patch-clamp recordings of HEK-293 T cells transfected with *hERG*(ΔAT), wild-type *hERG* (*hERG*(WT)), or both. The patient demonstrated an AT deletion (c.1735_1736del) in *hERG* and a decrease in

Y. Hata · K. Kinoshita · N. Nishida (✉)
Department of Legal Medicine, Faculty of Medicine, Graduate School of Medicine and Pharmaceutical Sciences for Research, University of Toyama, 2630 Sugitani,
Toyama 930-0194, Japan
e-mail: nishida@med.u-toyama.ac.jp

H. Mori · A. Tanaka
Department of Molecular Neuroscience, Graduate School of Medicine and Pharmaceutical Sciences for Research, University of Toyama, 2630 Sugitani,
Toyama 930-0194, Japan

Y. Fujita · T. Shimomura · T. Tabata
Laboratory for Neural Information Technology, Graduate School of Sciences and Engineering, University of Toyama, 3190 Gofuku, Toyama 930-8555, Japan

Y. Yamaguchi
Second Department of Internal Medicine, Graduate School of Medicine and Pharmaceutical Sciences for Research, University of Toyama, 2630 Sugitani,
Toyama 930-0194, Japan

F. Ichida
Department of Pediatrics, Graduate School of Medicine and Pharmaceutical Sciences for Research, University of Toyama, 2630 Sugitani,
Toyama 930-0194, Japan

Y. Kominato
Department of Legal Medicine, Graduate School of Medicine, Gunma University, 3-39-22 Showa-machi,
Maebashi 371-8511, Japan

N. Ikeda
Department of Forensic Pathology and Sciences, Graduate School of Medical Sciences, Kyushu University,
3-1-1 Maidashi, Higashi-ku,
Fukuoka 812-8582, Japan

🖄 Springer

*h*ERG mRNA transcripts. HEK-293 T cells showed lower production and cell surface expression of hERG(ΔAT) compared with hERG(WT) protein. In addition, the hERG(ΔAT) protein failed to form functional channels, while the activation kinetics of functional channels, presumably consisting of hERG(WT) subunits, were unaffected.

Conclusion The ΔAT mutation may decrease the number of functional hERG channels by impairing the posttranscriptional and posttranslational processing of the mutant product. This decrease may partly explain the cardiac symptoms of the patient who was heterozygous for *hERG*(ΔAT).

Introduction

Long QT syndrome (LQTS) is a congenital disorder that predisposes patients to sudden cardiac death (SCD) [1, 2]. The phenotypic and genetic heterogeneity of LQTS are widely accepted. The clinical history and electrocardiographic phenotype of LQTS can range from complete absence of symptoms and a normal resting electrocardiograph (ECG) to sudden death in infancy resulting from extreme QT prolongation [3]. Such phenotypic variability can make clinical diagnosis challenging. To date, LQTS has been attributed to mutations in 13 genes [4, 5]. Approximately 90 % of genotyped LQTS patients belong to type 1 LQT (LQT1), LQT2, or LQT3. LQTS has been shown to be an ion channelopathy associated with loss-of-function mutations in genes encoding repolarizing potassium channels, their subunits, and certain interacting proteins. Gain-of-function mutations in genes encoding depolarizing sodium and calcium channels have also been associated with LQTS [6]. LQTS-associated genes are listed in Table 1.

Nearly 300 LQT2-linked missense, frameshift, deletion, insertion, and nonsense mutations of the human *ether-à-go-go*-related gene (*hERG*) have been identified. *hERG* mutations can cause channel malfunction via diverse mechanisms, including abnormal channel protein processing, generation of nonfunctional protein, dominant-negative suppression, and alterations in channel gating [7]. More than 30 % of the *hERG* mutations identified are nonsense/frameshift mutations that introduce premature termination codons. These nonsense/frameshift mutations are more frequently located in the C-terminal region of the hERG protein and less frequently in the transmembrane pore domain (S5–loop–S6) [8].

Here we report a novel *hERG* frameshift mutation in the S5-pore region (*hERG*(ΔAT)), identified during LQTS genetic screening of a patient who died from SCD. This patient displayed only mild corrected QT interval (QTc) prolongation during electrocardiography and had no prior symptoms. We also evaluated the *hERG* transcript level in the patient's blood. To elucidate the pathogenic mechanism of hERG(ΔAT), we examined the molecular and electrophysiological behaviors of the protein product by performing immunoblotting, immunocytochemistry, and patch-clamp recordings of hERG-transfected HEK-293 T cells.

Materials and methods

Subject characteristics

A 44-year-old woman died suddenly 10 h after awakening from general anesthesia for microscope-guided resection of a laryngeal granuloma. The histology of the extirpated specimen showed that it was nonspecific granuloma tissue. No neoplastic change, epithelioid granulomas, nor pathogens were found. Twelve-lead ECGs were obtained during the patient's preoperative examination. QT and RR intervals were measured on three consecutive sinus complexes in lead V_5. The QT value was corrected for heart rate according to Bazett's formula (QTc). The ECG demonstrated a prolonged QTc interval of 493 ms, but the patient had no clinical history of cardiac symptoms, such as syncope, near-syncope, or palpitations. No family history was available either. An autopsy was performed to clarify the cause of death. At autopsy, the heart weighed 320 g and was examined both macroscopically and microscopically using methods previously reported [9]. The heart showed mild dilatation of the left atrium and ventricle, mild thinning of the left ventricular walls, and hypertrabeculation of the papillary muscle of the left ventricle (Fig. 1a, b). The thickness of the anterior wall of the left ventricle, ventricular septum, and right ventricle was 1.3, 1.2, and 0.2 cm, respectively. The mitral leaflet was thickened and showed mild myxoid degeneration. The coronary arteries were normal in appearance. Histological specimens were taken from one or two circumferential horizontal sections at the levels of the papillary muscle and apex. The sinoatrial node and atrioventricular conduction systems were also examined. Histologically, the patient had above average degrees of interstitial fibrosis for her age in the left ventricle (Fig. 1c) and in the atrioventricular conduction system. No other clinically significant lesions were found, and these cardiac abnormalities were deemed insufficient to be the cause of death.

A control subject, a 36-year-old man, was heterozygous for a synonymous polymorphism (1692A/G) in *hERG* (*hERG*(L564L)) and lacked mutations in any other major arrhythmia-related genes. This control was used for analysis of mRNA isolated from whole blood.

Table 1 Genes associated with long QT syndrome

| Gene	Type	Protein	Functional effect
KCNQ1	LQT1	I_{Ks} potassium channel α-subunit	Loss-of-function
hERG (KCNH2)	LQT2	I_{Kr} potassium channel α-subunit	Loss-of-function
SCN5A	LQT3	I_{Na} sodium channel α-subunit	Gain-of-function
ANK2	LQT4	Ankyrin B, anchoring protein	Loss-of-function
KCNE1	LQT5	I_{Ks} potassium channel β-subunit	Loss-of-function
KCNE2	LQT6	I_{Kr} potassium channel β-subunit	Loss-of-function
KCNJ2	LQT7	I_{K1} potassium channel α-subunit	Loss-of-function
CACNA1C	LQT8	I_{Ca} calcium channel α-subunit	Gain-of-function
CAV3	LQT9	Caveolin	Loss-of-function
SCN4B	LQT10	I_{Na} sodium channel β-subunit	Loss-of-function
AKAP9	LQT11	Yotiao, A-kinase-anchoring protein	Loss-of-function
SNTA1	LQT12	α1-Syntrophin	Loss-of-function
KCNJS	LQT13	Kir3.4 subunit of I_{KAch} channel	Loss-of-function

Genetic analysis

Genomic DNA was extracted directly from whole blood using a QIAamp DNA Blood Mini Kit (Qiagen Science, MD, USA). Genomic DNA samples were PCR-amplified using primers designed to amplify the complete sequences of all five major arrhythmia-related genes [i.e., *KCNE1* (GenBank accession number, NM_00219.4), *KCNE2* (NM_172201.1), *KCNQ1* (NM_000218.2), *SCN5A* (NM_000335.4), and *hERG* (NM_000238.3)], cardiomyopathy-associated sarcomere genes [i.e., *MYH7* (NM_000257.2), *MYBPC3* (NM_000256.3), *TNNT2* (NM_000364.2), *ACTC1* (NM_005159.4), and *TPM1* (NM_001018005.1)], and desmosome genes [i.e., *PKP2* (NM_004572.3), *DSP* (NM_004415.2), *DSG2* (NM_001943.3), *JUP* (NM_002230.2), and *DGC2* (NM_024422.3)] [10]. The nucleotide sequences of the

amplified fragments were analyzed by direct sequencing in both directions using the BigDye Terminator v3.1 Cycle Sequencing Kit (Applied Biosystems, CA, USA). Sequence analysis was performed using the ABI PRISM 3100-Avant Genetic Analyzer (Applied Biosystems). In addition, PCR products were subcloned into the pCR2.1 plasmid vector (Invitrogen, CA, USA).

Reverse transcription-PCR (RT-PCR)

Total RNA was isolated from whole blood that had been stored at −80 °C, and RT-PCR was performed as previously described [11]. *hERG* mRNA was reverse-transcribed and amplified using primers corresponding to sequences in exons 6 and 7 (Fig. 3). The sequences of the primers were as follows: Ex6F—5′ ACT ACT TCA AGG GCT GGT TCC TCA TCG 3′ and Ex7R—5′ AGT AGA GCG CCG

Fig. 1 Gross and microscopic appearance of the heart. **a, b** Horizontal sections of the ventricles. Hypertrabeculation of the left ventricle, especially the apex, was evident. **c** Left ventricle. Moderate fibrosis and endocardial thickening were present. Scale bar=100 μm
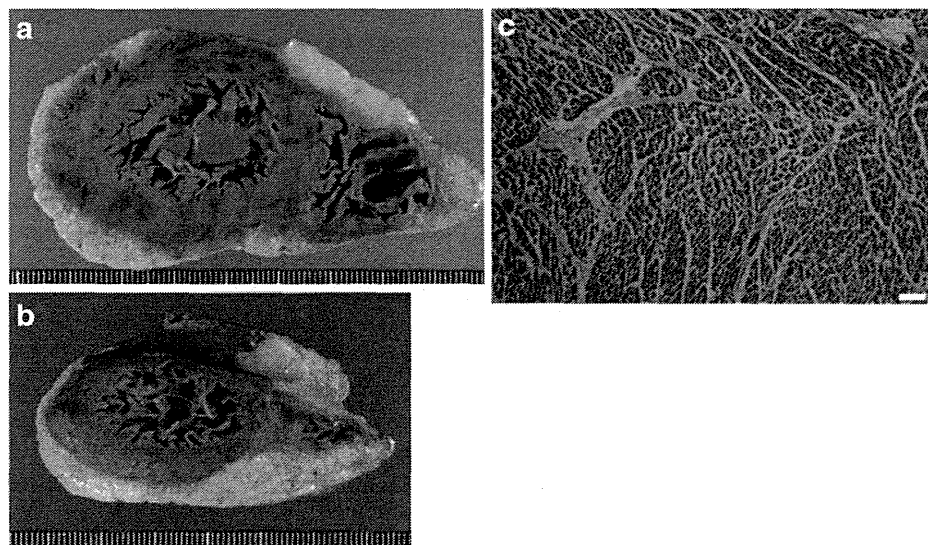
TCA CAT ACT TGT CC 3'. PCR cycling conditions were 94 °C for 1 min; 40 cycles of 94 °C for 1 min, 60 °C for 1 min, and 72 °C for 1 min; and 72 °C for 5 min. PCR amplifications were performed in 25 μL reaction mixtures containing 5 pmol of each primer, 1.3 U of *Ex Taq* DNA polymerase (Takara Bio Inc., Shiga, Japan), 200 μM dNTPs, and 1× GC buffer I (Takara). The amplified fragments were sequenced as described above.

Construction of hERG(WT) and hERG(ΔAT) expression vectors

The pSI-*hERG* expression vector [12] was kindly provided by Drs. Kenshi Hayashi (Kanazawa University Graduate School of Medical Science, Kanazawa, Japan) and Sabina Kupershmidt (Vanderbilt University, School of Medicine, Nashville, TN, USA). pSI-*hERG* was digested with *Bam*HI, followed by ligation with a linker DNA fragment containing *Bam*HI–*Sal*I–*Bam*HI sites to yield the plasmid pSI-*hERG*-BSB. The 1.4-kb fragment obtained after digesting pSI-*hERG* with *Xho*I and *Sal*I was subcloned into the *Xho*I site of the expression plasmid pCAGGS [13], which was a kind gift from Dr. Jun-ichi Miyazaki (Osaka University Medical School, Osaka, Japan), to construct the plasmid pCAG-*hERG*-XS. The 2.1-kb fragment obtained after digesting pSI-*hERG* with *Xho*I was subcloned into the *Xho*I site of pBluescript II (Clontech Laboratory Inc., CA, USA) to generate pBS-H-Xh2.1. The 266-bp DNA fragment containing the ΔAT mutation was constructed through two-step PCR [14] using the appropriate primers and pBS-H-Xh2.1 as a template, followed by digestion with *Nhe*I and ligation with *Nhe*I-digested wild-type pBS-H-Xh2.1 to yield plasmid pBS-H-Xh2.1-ΔAT. The 2.1-kb fragments of *hERG*(WT) and *hERG*(ΔAT), obtained from *Xho*I digestion of pSI-*hERG* and pBS-H-Xh2.1-ΔAT, respectively, were subcloned individually into the *Xho*I site of pCAG-*hERG*-XS to construct the expression vectors pCAG-*hERG*(WT) and pCAG-*hERG*(ΔAT), respectively.

DNA fragments encoding double hemagglutinin (HA) tags (GGG GSY PYD VPD YAG GGG SYP YDV PDY A) or double myelocytomatosis viral oncogene (Myc) tags (GGG GSA SMQ KLI SEE DLG GGG SAS MQK LIS EED L) flanked by linkers were prepared by annealing the appropriate oligonucleotide DNAs. The HA-tag was attached to the C-terminus of *hERG*(WT) and the Myc-tag to the C-terminus of *hERG*(ΔAT) through the inverse PCR method [15], using a KOD-plus mutagenesis kit (Toyobo, Tokyo, Japan). The 1.1-kb *Sac*I–*Hin*dIII fragment containing the HA-tag was replaced with the *Sac*I-*Hin*dIII-digested fragment of *hERG*(WT) to yield HA-tagged *hERG*(WT). The 1.2-kb *Bst*EII–*Sph*I fragment containing the Myc-tag was replaced with the *Bst*EII–*Sph*I fragment of *hERG*(ΔAT) to yield Myc-tagged *hERG*(ΔAT).

Cell culture and DNA transfection

Human embryonic kidney (HEK) 293 T cells (no. CRL-11268, American Type Culture Collection, VA, USA) were grown in Dulbecco's modified Eagle's medium supplemented with 10 % fetal bovine serum and 0.5 % penicillin–streptomycin at 37 °C and 5 % CO_2. Briefly, 2.0×10^5 HEK-293 T cells were seeded into a 35-mm dish the day before transfection. Construct plasmid DNA was added onto the cell monolayer (0.5 μg for Western blot analysis; 225 ng for patch-clamp recordings; or 1 μg for immunocytochemistry), as well as 10 μL TransIT-293 transfection reagent (Mirus, WI, USA) in 1 mL Dulbecco's modified Eagle's medium, according to the manufacturer's instructions. The p*EGFP*-N1 vector (Clontech) encoding enhanced green fluorescent protein (GFP) was co-transfected with the plasmid construct, and the target cells were identified by fluorescence microscopy. At 48 h post-transfection, the cells were scraped from the plates for Western blotting, fixed according to standard protocols for immunocytochemistry, or trypsinized as standards for patch-clamp recordings.

Western blotting

After the 48-h incubation, HEK-293 T cells transiently transfected with *hERG*(WT) and *hERG*(ΔAT) were washed with phosphate-buffered saline (PBS; pH 7.4), homogenized in mammalian protein extraction reagent (M-PER, Thermo Scientific, IL, USA), and centrifuged at 17,800×*g* for 10 min. Protein concentrations in the supernatants were determined using the BCA Protein Assay Kit (Thermo Scientific). The extracted protein samples were heat-denatured, electrophoresed in 7.5 % sodium dodecyl sulfate-polyacrylamide gels, and transferred to a polyvinylidene difluoride membrane (GE Healthcare, Tokyo, Japan). The membrane was blocked with 5 % skim milk in Tris-based buffer (TBS; 20 mM Tris–HCl, pH 7.6, 137 mM NaCl) containing 0.1 % Tween-20 (TBST) for 1 h. The polyclonal anti-hERG antibody (Santa Cruz Biotechnology, CA, USA) used in the present study was raised in rabbits against amino acids 96–270, which lie near the N-terminus of human hERG. The membrane was incubated with rabbit anti-hERG antibody (1:200 dilution) overnight at 4 °C, washed the next day in TBST, and incubated with a secondary antibody (1:10,000 dilution; goat anti-rabbit IgG HRP, Bio-Rad, Tokyo, Japan) at room temperature for 1 h. The membrane was washed again in TBST, and protein bands were detected using the ECL Prime Western Blotting Detection System (GE Healthcare) with a lumino-imaging analyzer (ImageQuant LAS-4000, Fujifilm, Tokyo, Japan).

Immunocytochemistry and confocal microscopy

HEK-293 T cells (2.5×10^5 cells per dish) were seeded on polyethyleneimine-coated 35 mm glass-based dishes (Iwaki, Chiba, Japan). After 24 h of incubation, the cells were co-transfected with the plasmids HA-tagged *hERG*(WT) and Myc-tagged *hERG*(ΔAT). The cells were cultured for 48 h, fixed in 4 % paraformaldehyde for 10 min at room temperature, permeabilized with 0.1 % Triton X-100 in PBS for 5 min, and then incubated in blocking solution (PBS containing 5 % goat serum) for 30 min. Subsequently, the cells were incubated overnight in PBS containing rat monoclonal anti-HA antibody (1:800 dilution; Roche Diagnostics, IN, USA) and rabbit polyclonal anti-Myc antibody (1:125 dilution, Santa Cruz Biotechnology) at 4 °C. The next day, the cells were washed in PBS and incubated with goat anti-rat IgG Alexa Fluor 568 (1:500 dilution; Invitrogen) and goat anti-rabbit IgG Alexa Fluor 647 (1:500 dilution; Invitrogen) at room temperature for 1 h. The cells were washed in PBS, and the nuclei were stained using 4',6-diamidino-2-phenylindole. Images were obtained by confocal laser microscopy (TCS SP5, Leica, IL, USA).

Electrophysiology

Ruptured-patch whole cell voltage-clamp recordings were performed. A recording pipette was pulled from a glass capillary to a tip resistance of ~5 MΩ and filled with a solution comprising 134 mM potassium D-gluconic acid, 7.6 mM KCl, 9 mM KOH, 10 mM NaCl, 1.2 mM MgCl$_2$, 10 mM HEPES, 0.5 mM EGTA, and 4 mM ATP magnesium salt (pH adjusted to 7.3 with D-gluconic acid). The recording bath was perfused at a rate of 0.7 mL/min with 147 mM NaCl, 3 mM KCl, 2 mM CaCl$_2$, 1 mM MgCl$_2$, 10 mM HEPES, and 10 mM D-glucose (pH adjusted to 7.4 with NaOH). The command voltages were corrected for the liquid junction potential between the pipette and bath solutions. Current signals were acquired using an EPC 9 Double amplifier (HEKA, Lambrecht, Germany; cut-off frequency 2 or 5 kHz; sampling frequency 5 or 50 kHz) that was controlled using Pulse software (version 8.53; HEKA). The holding voltage was −80 mV.

After a recording configuration was established, the pipette capacitance was canceled electronically, and current responses to 10 bipolar voltage pulses (amplitude ±5 mV; duration 40 ms) were recorded. The cell membrane capacitance (C_m) was then canceled electronically, and whole cell currents were recorded at an electronic series resistance compensation of 60 %. After the recordings, the passive cell membrane conductance and C_m were estimated from the average of the pulse-evoked current responses and

used for off-line linear leakage subtraction and calculation of the current density (i.e., current amplitude per unit C_m). Function fitting to the data were performed using JMP software (version 7.0.2, SAS Institute, NC, USA). To evaluate the voltage dependence of activation, a Boltzmann equation ($I_{hERG} = A/[1 + (V_{half} - V_{comm})/K]$, where I_{hERG}, A, V_{half}, V_{comm}, and K are the amplitude of hERG channel current, scale factor, voltage for half-maximal activation, command potential, and slope, respectively) was fitted to the current density-command potential plot for each cell. The time constant was estimated from the single-exponential curve fitted to the rising phase (a range of first-step duration from zero to the point at which the activation extent became saturated) of the plot of activation extent against first-step duration (cf. Fig. 6d) for each cell.

Data from numerical data groups are presented as mean± SEM. Significant differences (i.e., $P < 0.05$) between numerical data groups were evaluated using the van der Waerden rank-sum test because the majority of the groups were judged to have non-normal distribution according to the Shapiro–Wilk test.

Results

Genetic studies

Among major arrhythmia-related genes including *KCNE1*, *KCNE2*, *KCNQ1*, *SCN5A*, and *hERG*, only *hERG* demonstrated any mutation—in this case, a heterozygous AT deletion (c.1735_1736del), which gave rise to the mutant gene *hERG*(ΔAT) (Fig. 2a). This deletion changes the amino acid at position 579 and causes a shift in the reading frame resulting in the generation of a premature stop codon at amino acid 653 (p.M579fs+75X). The deletion therefore creates a new amino acid sequence between position 579 and 74 residues downstream, instead of the C-terminal 581 amino acids that occur in the WT protein (Fig. 2b). This allele therefore encodes a truncated protein that lacks the pore-S6 region and the C-terminus (Fig. 2c). Because amino acids 579–1159 (which comprise the S5-pore region and C-terminus of hERG) include domains required for appropriate tetramerization, maturation, stability, and surface expression of hERG channels [7], this AT deletion may lead to a loss-of-function mutant protein. Within the desmosome genes (*PKP2*, *DSP*, *DSG2*, *JUP*, and *DSC2*) sequenced, two previously published nonsynonymous polymorphisms [16] were also identified, one in *DSP* (p.R1738A) and the other in *JUP* (p.M697L). No mutations were found in *PKP2*, *DSG2*, or *DSC2*. We did not identify any mutations in the sarcomere genes (*MYH7*, *MYBPC3*, *TNNT2*, *ACTC1*, or *TPM1*).